Marine Geology 477 (2024) 107387

Contents lists available at ScienceDirect

Marine Geology

journal homepage: www.elsevier.com/locate/margo

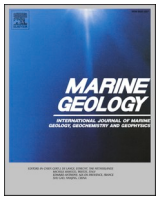

Japan Trench event stratigraphy: First results from IODP giant piston coring in a deep-sea trench to advance subduction zone paleoseismology

Michael Strasser [a,*], Ken Ikehara [b], Charlotte Pizer [a], Takuya Itaki [b], Yasufumi Satoguchi [c], Arata Kioka [d,e], Cecilia McHugh [f], Jean-Noel Proust [g], Derek Sawyer [h], IODP Expedition 386 Expedition Management Team, IODP Expedition 386 Expedition Science Party

[a] Department of Geology, University of Innsbruck, Innrain 52f 6020, Innsbruck, Austria
[b] Geological Survey of Japan, National Institute of Advanced Industrial Science and Technology (AIST), Tsukuba Central 7, 1-1-1 Higashi, Tsukuba, Ibaraki 305-8567, Japan
[c] Lake Biwa Museum, 1091 Oroshimocho, Kusatsu, Shiga 525-0001, Japan
[d] Department of Earth Resources Engineering, Graduate School of Engineering, Kyushu University, Nishi-ku, Fukuoka 819-0395, Japan
[e] Department of Systems Innovation, School of Engineering, The University of Tokyo, 7-3-1 Hongo, Bunkyo-ku, Tokyo 113-8656, Japan
[f] School of Earth and Environmental Sciences, Queens College, City University of New York65-30, Kissena Blv.Flushing, NY 11367, USA
[g] Géosciences-Rennes, CNRS, Université Rennes, Campus de Beaulieu, 35042 Rennes cedex, France
[h] The Ohio State University, School of Earth Sciences, 125 South Oval Drive Columbus, Ohio, 43210, USA

ARTICLE INFO

Editor: Michele Rebesco

Keywords:
Event stratigraphy
Hadal Trench Sedimentology
Paleoseismology
Core-to-seismic correlation
Giant piston coring
IODP
Japan Trench

ABSTRACT

The International Ocean Discovery Program (IODP) Expedition 386, Japan Trench Paleoseismology, represents the first utilization of giant piston coring (GPC) within scientific ocean research drilling. This allowed for a Mission Specific Platform (MSP) multi-site, multi-hole, shallow subsurface coring in an ultra-deep water subduction zone trench. The primary objective of the expedition was to investigate the concept of submarine paleoseismology in the Japan Trench, which involves studying long-term records of deposits in the deep sea that can provide insights into past earthquake events. In this paper, we compile and interpret initial shipboard data and results to (1) establish first-order event stratigraphic correlation of thick event beds (> 50 cm in thickness) between sites, (2) test previously published event-stratigraphic predictions of earthquake-related event deposits as proposed based on high-resolution hydro-acoustic subbottom profiler (SBP) data, and (3) derive SBP-scale event deposits age estimates to (4) discuss the advantages and limitations of giant piston coring for scientific drilling operations and the potential of new event stratigraphy results for advancing submarine paleoseismology.

The findings of the study identified a total of 77 SBP-scale event beds across 15 sites along a trench-parallel transect spanning over 600 km. These event beds exhibit clear expressions in SBP data, with approximately 49 % matching precisely with SBP units previously identified by Kioka et al. (2019a). For the remaining 51 % of SBP-scale event beds, thin, acoustically-transparent bodies were observed between high-amplitude horizons, for which SBP-based seismic interpretation alone would not be definitive. Consequently, the study concluded that the SBP-scale event-stratigraphy observed in IODP 386 cores validates the event-bed mapping conducted by Kioka et al. (2019a) and improves SBP interpretation for event beds in the 0.5 to 1 m thickness range.

The initial age constraints obtained from shipboard radiolarian biostratigraphy enable us to provide rough estimates of event ages by linearly interpolating between previously dated events occurring less than 2000 years ago and a datum around 11,000 years ago reported in four boreholes from trench basins in the Southern, Central, and Northern Japan Trench. Inter-site stratigraphic correlation reveals distinct SBP-scale event stratigraphies for the trench segments located to the north and south of the structurally complex "boundary area" at approximately 39.3–39.4°N, which is hypothesized to potentially act as a persistent rupture barrier for megathrust earthquakes. We observe more frequent but thinner event deposits in the Southern and Central Japan Trench, and fewer but thicker event beds in the Northern Japan Trench. This spatial variation may be related to the different seismogenic behavior of the various asperities along the Japan Trench megathrust and/or to differences in the response of slope sediments to earthquake shaking. However, here-presented investigations at the SBP-scale level are deemed too simplistic for robust application of the "submarine paleoseismology" approach. The extensive

* Corresponding author.
E-mail address: michael.strasser@uibk.ac.at (M. Strasser).

https://doi.org/10.1016/j.margeo.2024.107387
Received 24 March 2024; Received in revised form 15 July 2024; Accepted 24 August 2024
Available online 28 August 2024

and high-quality dataset from IODP GPC, coupled with the encouraging initial correlation results presented here, leads us to hypothesize that further detailed studies can identify and characterize event deposition dynamics at the micro-facies level, refine sediment provenance, and constrain precise event ages necessary for evaluating synchronicity in paleoseismological interpretation. These studies will also enable robust exploration of along-strike correlations or variations, facilitating the extraction of paleo-earthquake signals from Japan Trench event stratigraphies.

1. Introduction

The deepest oceanic realms on Earth are in hadal (>6000 m water depth) trenches, formed by the downward bending of the oceanic lithosphere in plate convergent settings (e.g., Kioka and Strasser, 2022). Here, most of the stresses accumulated by global plate tectonics are released by episodic subduction earthquakes with often devasting consequences (e.g., Bilek and Lay, 2018). Understanding subduction zone processes in hadal trenches as one of the least explored aquatic environments on Earth represents new frontiers for marine geology research (e.g., Jamieson et al., 2010; Kioka and Strasser, 2022; Ueda et al., 2023 and references therein). As a result of the technological challenges in surveying and subseafloor sampling in such great water depths, hadal oceanic trenches are also arguably one of Earth's most challenging environments for scientific ocean drilling research. Forty-three years ago, the legendary Drilling Vessel (D/V) *Glomar Challenger* set a long-standing record for the deepest coring site sampled by scientific ocean drilling, recovering two 15.5 m and 20.5 m long cores from water depths 7034 and 7029 m below sea level (mbsl) in the Mariana Trench (Site 461) during Deep-Sea-Drilling-Program (DSDP) Leg 60 (Hussong et al., 1982). In 2021, International Ocean Discovery Program (IODP) Expedition 386 broke this record by recovering 29 long cores of up to 37.82 m from 15 sites located at water depths between 7445 and 8023 mbsl in the Japan Trench (Ikehara et al., 2023; Strasser et al., *2023*). This success was facilitated by Mission Specific Platform (MSP) Giant Piston Coring (GPC) from Research Vessel R/V *Kaimei*, which for the first time in 50 years of scientific ocean drilling, enabled efficient multi-site, multi-coring subsurface sampling in ultra-deep water hadal environments (McInroy et al., *2024*).

At the Japan Trench, the devastating impact of the 2011 Tohoku-oki megathrust earthquake sparked a tremendous international research effort to better understand the causes, effects, and frequency of subduction zone earthquakes (e.g., Uchida and Bürgmann, 2021; Kodaira et al., *2021* and reference therein). However, current observational data series are too short to fully capture the complete spectrum of spatial and temporal variability of megathrust slip behavior (Wirth et al., *2022*). Longer observations that span multiple seismic cycles are required to conclusively reveal whether earthquake behavior has predictable cyclic recurrence characteristics (Moernaut, J., 2020) and whether patterns of fault coupling, and rupture barriers are persistent (Daigle et al., 2023 and references therein). Over the last decade, several research efforts have focused on surveying, sampling and studying hadal trench-fill basins hypothesized to act as terminal sinks for earthquake-triggered submarine sediment-gravity flows and thus may record stratigraphic evidence of past megathrust earthquakes (e.g., Ikehara et al., *2016, 2021*; Kanamatsu et al., *2022, 2023*; Usami et al., 2018; Oguri et al., 2013; McHugh et al., 2020; Kioka et al., 2019a, 2019b; Schwestermann et al., 2020; Strasser et al., 2013*)*. IODP Expedition 386 was motivated to explore 'submarine paleoseismology' at the Japan Trench to generate a multi-millennial record of giant (~ Magnitude(M)9 class[1]) subduction zone earthquakes, such as the 2011 Tohoku-oki earthquake (Ikehara et al., 2023; Strasser et al., *2023*).

The 'submarine Paleoseismology' approach combines spatiotemporal mapping of earthquake-related event deposits in the continuous deep sea sedimentary record to define past rupture limits and statistical analyses of earthquake recurrence patterns along subduction margins (e.g., Goldfinger et al., 2012; Moernaut, J., 2020; Walton et al., *2021*). The approach is underpinned by the assumptions that (1) there is a predictable relation between earthquake rupture characteristics, ground-motion-induced sediment remobilization, margin-physiography-controlled sediment transport and event-layer deposition; and (2) that synchronicity can be established from sedimentological and geochronological data (e.g., Howarth et al., 2021).

Currently available data sets for subduction zone submarine paleoseismology have mostly been limited by conventional 10 m long coring (see compilations by De Batist et al. (2017), Howarth et al. (2021), and references therein). These cores often only comprise a few seismoturbidites that do not fully capture the complete spectrum of spatial and temporal variability of megathrust slip behavior and earthquake-triggered sediment remobilization processes. Yet, they are mostly spatially extensive, allowing for assessment of stratigraphic correlation of event beds based on multiproxy signature between widely separated sites and for positive correlation to instrumental and historic earthquakes. For several subduction margins, state-of-the-art submarine paleoseismology research hence has achieved qualitative and in places even quantitative calibration of the "submarine event-bed paleoseismometer" (e.g., Goldfinger et al., 2012; Ikehara et al., *2016*; Polonia et al., 2017; Kioka et al., 2019a, 2019b; Howarth et al., 2021).

As demonstrated by pioneering studies using the CALYPSO coring system, inferred earthquake-related event deposits can be tracked further back in time by sampling longer sedimentary sequences using giant piston coring technique (Grácia et al., 2010; Pouderoux et al., 2014; Seibert et al., *2024; and* St-Onge et al., 2012). However, application of the submarine paleoseismology approach on such long temporal records (i.e., reaching back in time to sample several low-recurrence events) still requires spatially extensive records that sample different types of events over long distances at locations with different flow accumulation to test the robustness of seismic event interpretation. Since feedback between earthquake type, seafloor motion, and its eventual manifestation in the stratigraphic record are complicated, no single proxy-technique can provide the full paleoseismic history at an individual site (Goldfinger et al., 2012; Howarth et al., 2021). Hence, submarine paleoseismology requires comprehensive, margin-wide, multi-site, long-term (i.e., deep subsurface) records to be studied by a broad range of disciplines, the results of which need to be integrated temporally and spatially. Efficiently coring and comprehensively deciphering such long records from deep water environments such as subduction trenches poses technological, logistical as well as scientific challenges, that are difficult to be addressed by smaller research groups on national levels.

IODP Expedition 386 addressed these challenges at the Japan Trench (Ikehara et al., 2023; Strasser et al., 2023). There, the assumptions behind the `submarine paleoseismology´ approach were initially validated by examining the sedimentary deposits from the most recent magnitude (M) 9 earthquake in 2011 (e.g., Strasser et al., 2013; Kioka et al., 2019b; Ikehara et al., *2021*). In the deepest trench-basins of the southern and central Japan Trench, these are several decimetres to

[1] we acknowledge that quantitative reconstruction of paleo-magnitudes to distinguish "giant" (M > 9) from "great", but still in the high M8++ range, is impossible. We here follow terminology used in recent literature despite its potential overstatement and also use "giant" for M9-type (similar to 2011 Tohoku-oki earthquake), for which M might actually also has been in the high M8++ range.

meter thick, mostly fine-grained sediment gravity flow deposits, imaged in high-resolution hydro-acoustic subbottom profiler (SBP) data by distinct, acoustically-transparent bodies with ponding geometries (Kioka et al., 2019a). Subsequently, key methodology was developed to reliably recognize, map, and date event deposits in the sediment spanning the last 1500 years and correlate them to the occurrence and distribution of known historical megathrust earthquakes (Ikehara et al., *2016*; Ikehara et al., 2017a; Bao et al., 2018; Kioka et al., 2019b; McHugh et al., 2020; Schwestermann et al., 2020, *2021*; Kanamatsu et al., *2022, 2023*). This resulted in the initial "calibration of the marine event-deposit paleoseismograph" in the Japan Trench (see more details section 2.2 below).

Importantly, the prior development of submarine paleoseismology at the Japan Trench provided the foundational knowledge and site survey data required to test and apply the approach on even greater spatial and temporal scales accessible only by deeper coring systems. In 2021–2023, this goal was realized by IODP Expedition 386, on which 29 giant piston cores were recovered at 15 sites along a trench-parallel transect spanning ~600 km of the Japan Trench subduction zone. This achievement not only constitutes the first research expedition to perform deep-subsurface (>10 m below sea floor; mbsf) and high spatial resolution sampling of a hadal oceanic trench but also, the first coordinated multidisciplinary international research effort investigating sedimentary event beds recorded in marine archives to test for earthquake origin and long-term earthquake magnitude – frequency relation (Ikehara et al., 2023; Strasser et al., *2023*).

In this paper, we compile and interpret IODP Expedition 386 initial shipboard data and results to (1) establish first-order event stratigraphic correlation of thick event beds (i.e., > 50 cm in thickness) between sites, and (2) test previously published event-stratigraphic predictions of earthquake-related event deposits as proposed based on SBP data (Kioka et al., 2019a). We also aim at elaborating on the advantages and limitations of IODP giant piston coring and at discussing our results with respect to the potential for further analyses of the entire IODP data set to address overarching submarine paleoseismology objectives at the Japan Trench.

2. Regional setting

2.1. Japan Trench subduction zone, earthquake history and margin segmentation

Along the Japan Trench, the Pacific Plate is subducting beneath the Okhotsk plate at a rate of 8.0–8.6 cm/y (DeMets et al., 2010). Instrumental and likely complete historical records of tsunamigenic subduction earthquakes extend about 400 years into the past, with more sporadic accounts for the preceding millennium (written records and oral legends for the 869 CE Jogan, 1454 CE Kyotoku and 1611 CE Keicho events; Goto et al., 2019; Sawai, 2020 and references therein; CE = Common Era). Geological records documenting occurrence of large tsunamis preserved along the east-facing coast of Honshu span about 3000 years (to occasionally 5000 years; Goto et al., 2019, 2021; Sawai, 2020; Takada et al., 2016; Higaki et al., 2021; Nakanishi et al., *2022*; Ishizawa et al., *2022*; Fig.1).

The instrumental, historical, and geologic data clearly document along-strike and temporal variability in rupture mode for past earthquakes, suggesting that the recurrence interval of M9-type megathrust ruptures may be as short as 570 years (Philibosian and Meltzner, 2020). A "supercycle"[2] of giant earthquakes with a recurrence interval of ~600–700 years and superimposed on the cycle of great (M7–8) earthquakes has been proposed for the megathrust off Tohoku (here referred to as the Tohoku-asperity; Fig.1Ac; Satake, 2015). The occurrence of three giant earthquakes in the last 1500 years is consistent with return times of 260–880 years for M9-type earthquakes off Tohoku as calculated from seismic moment frequency *relation (*Uchida and Matsuzawa, 2011*),* and other recurrence estimates based on slip deficit accumulation over time assuming full interplate coupling (590–730 y; Uchida and Bürgmann, 2021) and seismo-mechanical modelling (520–800 y [Barbot, 2020]; ~600 y [Nakata et al., *2021*]).

From the available data, one might consider a potential persistent barrier around 39.3°N, separating the Tohoku asperities (approximate 2011 rupture area) from the Sanriku asperities in the north (Philibosian and Meltzner, 2020; Fig. 1). Yet, there appears to be separation between asperities along dip as well as along strike, and segmentation may not extend to the shallow domain of the megathrust, as the 1896 CE (and possibly 1611 CE) tsunami earthquakes appear to have traversed the Tohoku/Sanriku barrier. To the south of the 2011 rupture area, the Izu section seems to have less frequent earthquakes in general during the last 400 years (Philibosian and Meltzner, 2020). Earthquake rupture and the source of the Empo Boso-oki earthquake and tsunami of 1677 CE (Sawai et al., 2012), as well as an older tsunami-deposit dated about 1000 years ago, might also be explained by displacement on one of the other plate boundaries near the plate triple junction (Pilarczyk et al., *2021*).

Seismotectonics-based hypotheses have been presented to link the southern and northern rupture termination of the 2011 earthquake to structural heterogeneities in the overriding and subducting slab (e.g., *Bassett al., 2016*; Fujie et al., 2020). The impact of these features in and around the megathrust is thought to influence frictional properties, coupling and seismogenic behavior and therefore could represent potentially persistent rupture barriers. In the south, an abrupt SW-NE-striking boundary in upper-plate structure (black thick dashed linein Fig. 1) interpreted from gravity data, juxtaposes geological terranes composed of volcanic and plutonic rocks (in the north) and accretionary complexes (in the south) (Bassett et al., 2016). This contrast is suggested to explain the pattern of inter-seismic locking and giant earthquakes in the north (i.e., the Tohoku asperity) and interseismic creep and fewer or no giant earthquakes in the south (i.e., Izu section). In the north, recent magmatic intrusions and thermal metamorphism of the incoming pelagic sedimentary sequences overlying the down-bending Pacific oceanic crust has generated an area of 'petit-spot' volcanism at 39.3–39.4°N (Hirano et al., 2006). Fujie et al. (2020) suggest these features induce regional variations in friction along the megathrust preventing giant near-trench interplate coseismic slip. The trench floor along this part of the margin (herein referred to as "Boundary area between the Central and Northern Japan Trench") is also relatively shallower (~7400 m; as compared to ~7600, ~7500, and ~ 8000 mbsl in the northern, central, and southernmost parts, respectively), and high escarpment (>1 km) suggest large-scale gravitational collapse and mega-landslides on the lowermost landward slope (Nakamura et al., 2020, *2023*).

Slightly oblique subduction of N-S to NNW-SSE trending horst-and-graben structures formed by flexural bending of Pacific plate results in relatively rough trench-floor morphology with 0.5–15 km long and 0.5–5 km wide isolated trench-fill and graben-fill basins, with different along-strike connectivity (Figs. 1, 2a, b). Trench-basins in the central Japan Trench tend to be comparatively smaller (with basin areas defined as connected areas of flat seafloor <4 km^2) than those in the southern and northern trench (basin areas up 30 and 25 km^2, respectively (Kioka et al., 2019a, 2019b; Supplementary Table (Tab—S1). Trench basins represent the terminal depositional sinks for different sediment-gravity flow accumulation pathways (Fig. 2a; Kioka et al., 2019*a*), including those with and without upslope connectivity to shelf or coastal areas. The different lateral sediment transport systems from the upper slope into the trench are funnelled and can be reflected to form flow path

[2] The term "supercycle" is used in the literature for different types of cycle behavior in recurrence characteristics of major megathrust earthquake that have differing implications for fault mechanics and earthquake hazard. As addressing this is not the scope of this study, we here use the term as referenced in the respective cited study.

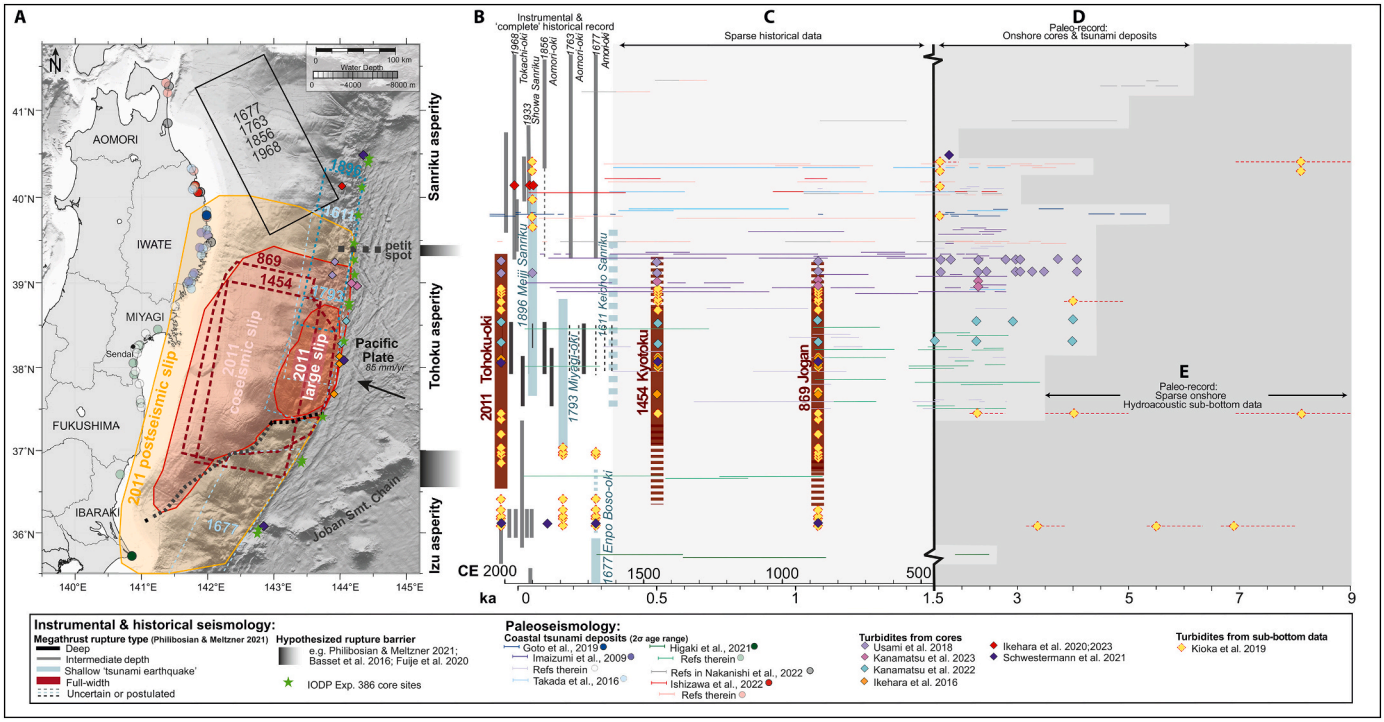

Fig. 1. Compilation of available earthquake and tsunami records of the Japan Trench Subduction Zone. A: Map modified after Kioka et al., 2019*a*, with schematic illustration showing the coseismic (red) and postseismic slip areas (orange) of the 2011 Tohoku-oki earthquake (*after* Uchida and Bürgmann, 2021); source areas of historically-known major (conceptually compiled from Nagai et al., 2001; Kanamori, 1971; Tanioka and Satake, *1996*; Takeuchi et al., 2007; Sawai et al., *2012,* 2015; Goto et al., *2019);* and geological structures (bold dashed black lines) hypothesized to be potential persistent barriers to giant megathrust ruptures (Philibosian and Meltzner, 2020; Bassett et al., 2016; Fujie et al., 2020*)*. Green stars mark IODP sites (this study, see Fig.2 for site number annotations); B to E: rupture history of the Japan Trench megathrust fault in space (y-axis = along-trench distance (same scale as A)) and time (x-axis = time) from historical (B, C) and geological (C, D, E) data. CE = Common Era; ka = calendar years before present (1950 CE); note change in relative scale at 1500 cal. BP. Time covered by (B) likely complete instrumental and historical, and (C) only sparse historical data. C, D, E divide the geological record into (C) calibrated by historical seismology; (D) covered by coastal tsunami records and offshore coring sites with high-resolution age constraints, and (E) not yet validated by state-of-the-art paleoseismologic research on cores (i.e., main target of this study). See legend for references, from which data was compiled. Where no range for age uncertainties is plotted, uncertainties are estimated to be smaller than symbol size. Note large dating uncertainties for coastal tsunami deposits compared to offshore paleoseismic event deposits, because of low determinative accuracy in low-sedimentation rate, often noncontinuous coastal sedimentary sequences (e.g., Ishizawa et al., *2022*). (For interpretation of the references to colour in this figure legend, the reader is referred to the web version of this article.)

systems along the trench axis for several tens of kilometres, connecting individual trench-slope basins. These systems are separated by bathymetric highs formed by the interconnection of different structural elements of the flexural-bended Pacific plate entering the subduction zone system (Fig. 2a, b).

2.2. *Previous studies of seismically-triggered event deposits at the Japan Trench*

A recent "boom" in submarine paleoseismology research at the Japan Trench has identified event beds resulting from earthquake-triggered sediment remobilization within basins along the slope and trench axis. Several thick (>50 cm) event beds are recognizable within sediment cores (extending back 2000–4000 years; refs) and as acoustically transparent bodies with ponding geometries in SBP data (extending <2000 years; refs). A variety of dating techniques has been used to successfully relate event beds in the uppermost sequences to historical earthquakes including the 2011 CE Tohoku-oki, 1454 Kyotoku and 869 Jogan, and extrapolation of sedimentation rates was used to postulate older events estimated to span >10,000 years (Kioka et al., *2019a*; Fig.1).

In particular, deposits generated by the 2011 earthquake, the subsequent tsunami and its aftershock sequence have been extensively studied using short-lived radionuclides (Oguri et al., 2013; McHugh et al., *2016*; Ikehara et al., *2016*; Kioka et al., 2019b) and transient disequilibrium pore water profiles (Strasser et al., 2013). The results indicate that the significant volumetric sediment transport to the trench is initiated by long-duration, low-frequency ground motion triggering the remobilization of just the uppermost few centimeters of young, unconsolidated, and fresh organic carbon (OC)-rich seafloor sediments over a very wide area, which roughly correlates with the megathrust rupture area (McHugh et al., *2016*; Kioka et al., 2019b; Molenaar et al., 2019; Schwestermann et al., 2020; Ikehara et al., 2020*)*. This results in characteristic, several decimetres to meter thick, mostly fine-grained homogenous sediment gravity flow deposits in the terminal basins of the 7–8 km deep Japan Trench. Examination of event deposits within cores from different trench basins show coherent event-internal multi-pulse stacking patterns that can be related to the flow accumulation of remobilized sediment in their respective upslope source areas (Figs. 1, 2; McHugh et al., *2016*, Ikehara et al., *2021*; Kioka et al., 2019a, 2019b; Schwestermann et al., 2021). No evidence for significant earthquake-related sediment remobilization is recorded in trench basins that are depositional terminal sinks of sediment gravity flows from upslope areas outside the 2011 rupture area (Kioka et al., 2019b). Likewise, the sediment-provenance- and flow-accumulation-inferred source areas for deposits related to the 1454 CE and 869 megathrust earthquakes correlate roughly with rupture areas reconstructed from coastal geologic evidence (*Kioka* et al.,2019b; Figs. 1, 2). Possible candidates for submarine event deposits related to historical shallow, near-trench "tsunami earthquakes" (e.g., 1896 CE, 1793, and 1611) were indicated by Usami et al. *(2018)* on the landward slope and by Kioka et al. (2019a) and Kanamatsu et al. *(2022, 2023)* suggesting possible

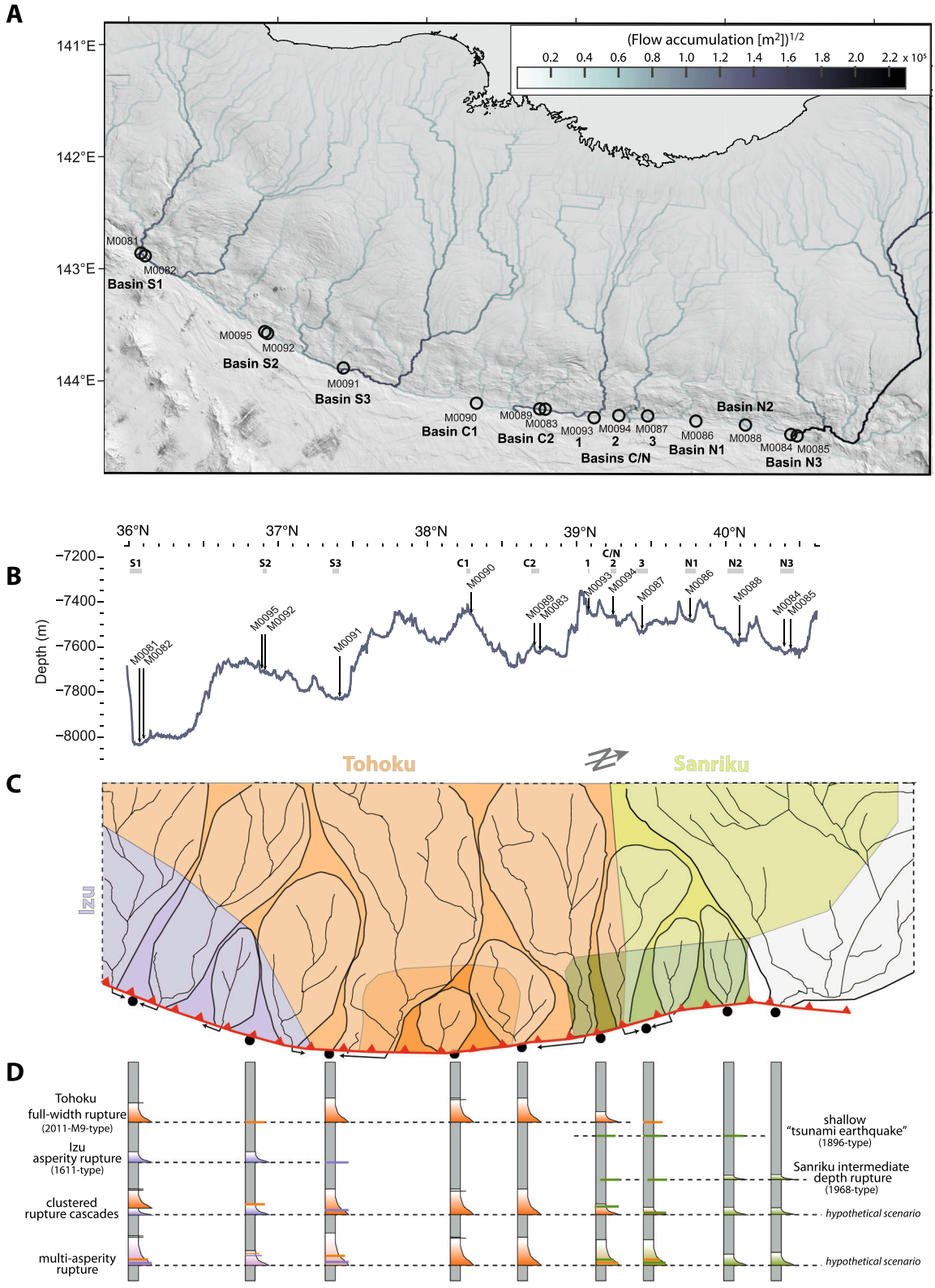

Fig. 2. Margin physiography and schematic of paleoseismology approach testing for event-stratigraphic correlation, source area identification, reconstruction of megathrust rupture area and distinguishing different types of hypothetical megathrust earthquake scenarios based on different stacking pattern in cores: (A) Flow accumulation map (illustrated as the square root of flow accumulation (m^2) and (B) along-trench bathymetric depth profile after Kioka et al. *(2019a)* with IODP Expedition 386 site locations *(*Strasser et al., *2023)* C) Schematic map based on (A) indicating source area of flow accumulation pathways relative to the main rupture areas for full-width vs. shallow depth megathrust ruptures along the Izu, Tohoku and Sanriku asperity (in light purple, orange and green, respectively; note that sketch is rotated relative to map (A) by 15 degree). (D*)* Schematic Core sections depicting the stacking pattern of deposits resulting from gravity flow from different source area, as "calibrated" for the different megathrust ruptures in historical times, and for two contrasting hypothetical extreme scenarios (clustered cascade vs. multi-asperity rupture). Note the fine tail from simultaneous multi-segment surficial slope sediment remobilization is expected to be mixed in the latter scenario. (For interpretation of the references to colour in this figure legend, the reader is referred to the web version of this article.)

correlation of thin event deposits in the trench-basins (Fig. 1), but conclusive information remains to be elaborated from cores with high spatial coverages.

3. Materials and methods

Event-stratigraphic correlation and interpretation is based on recently published IODP Expedition 386 data and results for which detailed methods are available in Strasser et al. (2023). In this paper, we uniformly compile lithostratigraphic, physical property and initial radiolarian biostratigraphy data for the longest Hole at each Site sampled by GPC during IODP Expedition 386 (Sites M0081 to M0095; Fig. 2). These data are used to systematically identify and characterize event beds with thicknesses resolvable within sub-bottom profile data at each site ('SBP-scale' event beds; section 3.2), and correlate these within and between different trench basins. The resulting first-order, margin-wide Japan Trench event-stratigraphy is then used to test the SBP-based event-stratigraphic prediction by Kioka et al. (2019a) and for discussing the potential of reconstructing comprehensive long-term earthquake histories along the entire subduction zone system.

3.1. Site locations and conceptual paleoseismology approach

IODP Expedition 386 was designed and implemented with coring site locations strategically optimized to overcome the challenges in validating the assumptions behind the submarine paleoseismology approach (Strasser et al., 2019). This involved targeting spatially well-constrained trench basins representing terminal depositional sinks for different sediment-gravity flow accumulation pathways (Fig. 2a). IODP Expedition 386 targeted 11 trench basins with source areas spanning across different margin segments (Fig. 2b). As a result, correlating cores from each basin should capture sediment remobilization triggered by earthquakes with a range of megathrust rupture scenarios (Fig. 2c).

For referring to the different basins in this study, we use the same basin annotation as Strasser et al. (2023), numbering trench basins with the prefix of the geographic location in the southern (S1–S3), central (C1 and C2), boundary area between the central and northern (C/N1–C/N3), and northern (N1−N3) Japan Trench. These locations are listed in Supplementary Table (Tab—S1) alongside the equivalent basin annotation used by Kioka et al. (2019a). Within each basin, one to three GPC-deployments recovered cores of the expanded stratigraphic section in the main depocenter. At strategically located focus basins, also the condensed stratigraphic section was sampled at the basin margin Sites (Fig. 2a; Tab—S1). This 'composite-stratigraphy concept' was utilized to (i) establish a robust stratigraphic pattern recognition for event interpretation; (ii) quantify variability on local and basin scales; (iii) minimize risk of sampling incomplete stratigraphy in one basin, and (iv) reach further back in time.

3.2. Event identification and discrimination between "SBP-scale" events, smaller events and hemipelagic pelagic background sediment

The identification of event deposits is based on interpretation of the sedimentary successions in the deepest Hole at each Site. For each of these 15 Holes, we integrate (i) line-scan images (including histogram-equalized images to enhance colour-specific facies variation), (ii) sagittal slice images of X-ray computed-tomography (CT) data, (iii) lithology defined by composition, structure and texture, and (iv) Multi-Sensor-Core-Logging (MSCL)-derived physical property data including magnetic susceptibility (MS), gamma-ray attenuation bulk density (density) and Natural Gamma Radiation (NGR) (see details on data acquisition methods in Strasser et al., 2023). Together, observations from these datasets (compiled for each Hole in Supplementary Figs. S1–15) are used to identify single event beds that result from deposition of waning sediment-gravity flows. Criteria to define the base of each event bed typically include (i) a sharp basal contact overlain by an overall fining-upward sequence, (ii) prominent peaks in physical property values that have asymmetric shapes with an abrupt base and upward-decreasing trends, and (iii) distinct radiodensity changes with comparable pattern resolved in three-dimensional X-ray CT data (Fig. 3a, d). Event bed tops are indicated by traces of bioturbation in structureless clay transitioning into burrow-mottled silty clays, typically exhibiting low magnetic susceptibility and bulk density values (Fig. 3a, b, f).

In some cases, multiple up to several cm-thick stacked sequences are observed near the top of thick event beds (Fig. 3a, b), which may correspond to either a single event sequence with multiple flows, or the superposition of multiple independent events shortly after each other. To remain objective, we classify each graded bed within stacked sequences as separate event beds. However, given the scope of this study which is to test first-order event-stratigraphic correlation of exclusively thick "SBP-scale" events, we only consider single event beds with a thickness of more than >50 cm. This value is 2.5 times the theoretical vertical resolution to the SBP data, and thus equivalent to an event bed that can be resolved by clear lateral pinch-out geometries of acoustically transparent facies against the acoustically laminated facies of "background" strata (Kioka et al., 2019a; note these authors picked the acoustic bodies that are thicker than 2 times the vertical resolution (~ 40 cm in depth converted SBP data), however the cores experienced significant elastic decompression and gas expansion so the depth scale of the cores is relatively expanded to the in situ depth imaged in SBP data (see discussion in section 5.1). This justifies the larger thickness threshold "SBP-scale" event deposits in the cores).

SBP-scale event deposits are numbered within each Hole from top to bottom and labelled according to the Hole and relative stratigraphic position of the thick deposit (TD) (e.g., M94B-TD4 is the fourth from top SBP-scale event deposit in Hole M0094B). Table 1 lists the top and bottom depth for each SBP-scale event deposit in meter below seafloor (mbsf = curated core depth scale of Strasser et al., 2023). Note that this depth scale does not correct for incomplete recovery of the first few decimetres to 2–3 m of the uppermost subseafloor section and coring disturbance, a common phenomenon for giant piston coring operations (e.g., Széréméta et al., 2004). It also does not account for core expansion/contraction because of gas expansion and elastic rebound and coring disturbance or artificial voids filled by foam at the top or bottom of the sections (see details in Strasser et al., 2023 and discussion in section 5.1).

3.3. Core-to-SBP correlation

P-wave velocity as a means to convert SBP two-way-travel time (TWT) to depth is not well constrained at each site due to the great water depth and may range between 1475 and 1950 m/s, as measured on cores by *Strasser* et al., (2023); obtained from velocity analysis in multi-channel reflection seismic data by Nakamura et al. *(2023)*; or estimated from SBP to shallow-subsurface core correlations by Kioka et al. *(2019a)*. Measurements on cores were impacted by expansion upon recovery from more than 7000 mbsl, as well as disturbance during storage, settling, transport and sampling. No velocity data is available from intervals with higher gas content (e.g., deeper than ~5–15 mbsf, (typically below the Sulfate-Methane-Transition Zone where increased gas content occurs; see discussion in section 5.1) because air between the liner and core reduced coupling and prohibited successful P-wave measurement (see supplementary figs. S1-S15; Strasser et al.,2023). Available MSCL-derived velocity data, however, reveals a positive correlation between bulk density and P-wave velocity data, suggesting that the continuously-measured density profile is a good proxy for impedance.

To compare and correlate the density profiles from cores with SBP data (see Kioka et al., 2019a for details on SBP acquisition, processing, and data resolution), we converted core-depth to TWT. However, given uncertainties in P-wave velocity data, we applied different velocities for

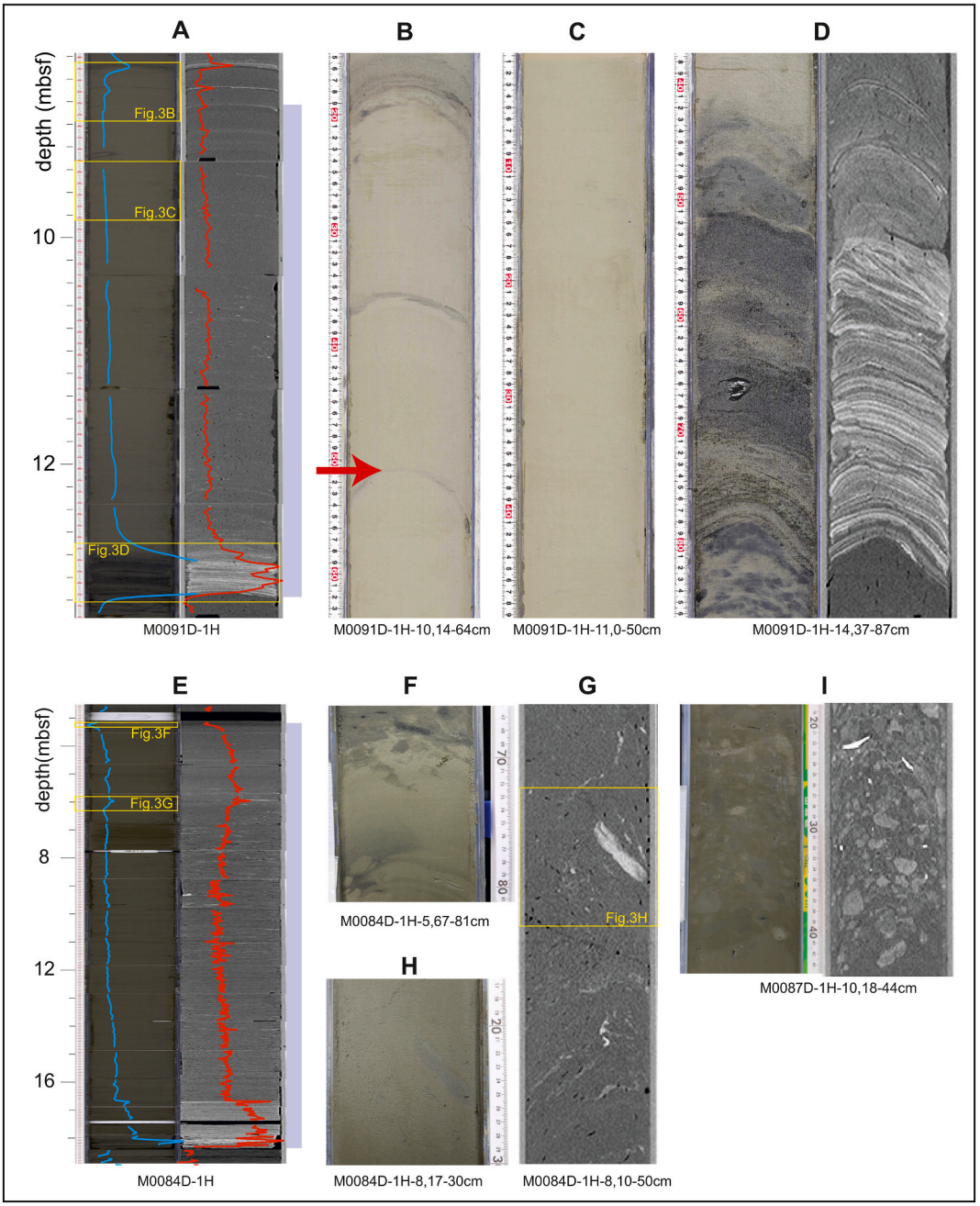

Fig. 3. Examples of event deposits: (A) linescan photo (left) and XCT image, with superimposed MSCL-derived relative MS (blue) and density (red) profiles, respectively, of SBP-scale event deposit M91-TD3. Yellow rectangles mark positions of zoomed-in contrast-adjusted line scan images showing (B:) Top of M91-TD3, marked with red arrow, and overlying multiple up to several cm-thick stacked sequences (see section 3.2 for definition and reasoning of defining event deposit top); (C): thick, structureless fine-grained interval lacking visible bioturbation (D): linescan (left) and XCT (right) images showing the basal sequence with a coarser (sandier) bed with sharp lower contact and grading upwards through (cross-)laminated and graded sand into overlying structureless interval (E) linescan photo (left) and XCT image, with superimposed MSCL-derived relative MS (blue) and density (red) profiles, respectively, of SBP-scale event deposit M84-TD1. Yellow rectangles mark positions of zoomed-in contrast-adjusted line scan images showing (F) burrow-mottled top and (G (XCT image); H (close-up core photo) soft-sediment deformation structures with floating silt and sand patches. (I): linescan (left) and XCT (right) images showing matrix (clay)-supported mud clasts with sub-rounded and irregular shapes. (For interpretation of the references to colour in this figure legend, the reader is referred to the web version of this article.)

different intervals in order to satisfy plausible visual SBP-to-core correlation. To do this, we first identified a series of prominent marker horizons in the cores (e.g., pronounced density peaks at the base of SBP-scale deposits) which easily correspond to high-amplitude reflections in SBP data. We then estimated the appropriate P-wave velocity for the interval between marker horizons, taking into account the absence of the uppermost sediments that are unrecovered by coring. As presented in section 4.2 (and further discussed in section 5.1) this approach reveals robust core-to-SBP correlation with velocities in the order of 1550–1600 m/s in the uppermost ~5–15 mbsf (and thus more consistent with the results from MSCL measurements), and increased velocities of 1650–1700 m/s in the lower parts (roughly consistent with P-wave velocity measurements on discrete samples; Strasser et al., 2023). Within >5 m thick event deposits, however, reasonable correlation often could only be achieved if the actual thickness of the interval within the core is assumed to be larger than the in-situ thickness of the respective interval

Table 1
SBP-scale event deposits.

Basin	Hole	SBP-scale event	Top core depth (m)	Bottom core depth (m)	Thickness (m)	Event-free depth (m)	Age estimate (ka) based on (1) event-free sed. rate (Datum 1/2 to Datum 3); (2) estimated age of correlative tie-point (Table 2); (3) on margin-wide average event free sed. Rate (2.25 mm/yr)	
Southern Japan Trench								
S1	M0081D	M81D-TD1	0.652	1.75	1.098	0.652	young than 869 CE	
		M81D-TD2	3.64	4.59	0.95	2.542	young than 869 CE	
		M81D-TD3	6.72	8.188	1.468	4.672	young than 869 CE	
		M81D-TD4*	8.795	12.888	4.093	5.279	1081 (869 CE)	
		M81D-TD5	12.965	13.625	0.66	5.356		1.12(3)
		M81D-TD6	13.94	15.125	1.185	5.671		1.26(3)
		M81D-TD7	20.205	21.465	1.26	10.751		3.51(3)
		M81D-TD8	23.12	23.77	0.65	12.406		4.25(3)
	M0082D	M82D-TD1	3.03	3.75	0.72	3.03	young than 869 CE	
		M82D-TD2*	4.17	5.03	0.86	3.45	1081 (869 CE)	
S2	M0095B	M95D-TD1	2.5491	3.444	0.8949	2.5491	young than 869 CE	
		M95D-TD2*	5.279	6.409	1.13	4.3841	1081 (869 CE)	
	M0092D	M92D-TD1	1.31	2.26	0.95	1.31	young than 869 CE	
		M92D-TD2	2.53	3.788	1.258	1.58	young than 869 CE	
		M92D-TD3	5.32	5.973	0.653	3.112	young than 869 CE	
		M92D-TD4*	6.032	8.709	2.677	3.171	1081 (869 CE)	
S3	M0091D	M91D-TD1	3.06	4.22	1.16	3.06	young than 869 CE	
		M91D-TD2	5.0737	5.94	0.8663	3.9137	young than 869 CE	
		M91D-TD3*	8.839	13.184	4.345	6.8127	1081 (869 CE)	
		M91D-TD4	17.566	18.913	1.347	11.1947		3.03(3)
		M91D-TD5	23.96	24.91	0.95	16.2417		5.27(3)
Central Japan Trench								
C1	M0090D	No SBP-scale event beds		–		–	–	
C2	M0089D	No SBP-scale event beds		–		–	–	
C2	M0083F	M83F-TD1	2.35	9.29	6.94	2.35	young than 869 CE	
		M83F-TD2*	11.18	15.44	4.26	4.24	1081 (869 CE)	
		M83F-TD3	19.57	20.095	0.525	8.37		2.78(2)
		M83F-TD4	25.2	26.335	1.135	13.475		5.29(2)
		M83F-TD5	26.9	27.77	0.87	14.04		5.55(2)
Central/Northern Japan Trench								
C/N1	M0093B	M93B-TD1	1.59	5.567	3.977	1.59		0.71(3)
		M93B-TD2	8.13	8.778	0.648	4.153		1.85(3)
		M93B-TD3	8.97	9.61	0.64	4.345		1.93(3)
		M93B-TD4	10.92	11.45	0.53	5.655		2.51(3)
		M93B-TD5	13.29	13.82	0.53	7.495		3.33(3)
		M93B-TD6	13.897	15.883	1.986	7.572		3.37(3)
		M93B-TD7	18.03	19.172	1.142	9.719		4.32(3)
		M93B-TD8	19.325	20.018	0.693	9.872		4.39(3)
		M93B-TD9	22.52	23.03	0.51	12.374		5.50(3)
		M93B-TD10	25.13	26.15	1.02	14.474		6.43(3)
C/N2	M0094B	M94B-TD1	0.359	1.094	0.735	0.359		0.16(3)
		M94B-TD2	1.448	2.23	0.782	0.713		0.32(3)
		M94B-TD3	2.57	3.38	0.81	1.053		0.47(3)
		M94B-TD4	3.46	4.409	0.949	1.133		0.50(3)
		M94B-TD5	4.48	10.735	6.255	1.204		0.54(3)
		M94B-TD6	11.47	11.99	0.52	1.939		0.86(3)
		M94B-TD7	12.251	12.79	0.539	2.2		0.98(3)
		M94B-TD8	12.87	13.84	0.97	2.28		1.01(3)
		M94B-TD9	14.165	15.117	0.952	2.605		1.16(3)
		M94B-TD10	15.86	18.264	2.404	3.348		1.49(3)
C/N3	M0087D	M87D-TD1	0.29	3.31	3.02	0.29		0.13(3)
		M87D-TD2	3.365	4.308	0.943	0.345		0.15(3)
		M87D-TD3	5.409	6.499	1.09	1.446		0.64(3)
		M87D-TD4	6.55	9.17	2.62	1.497		0.67(3)
		M87D-TD5	9.2	9.983	0.783	1.527		0.68(3)
		M87D-TD6	10.184	10.82	0.636	1.728		0.77(3)
		M87D-TD7	10.83	15.17	4.34	1.738		0.77(3)
		M87D-TD8	15.2	16.23	1.03	1.768		0.79(3)
		M87D-TD9	16.23	16.92	0.69	1.768		0.79(3)
		M87D-TD10	17.01	17.71	0.7	1.858		0.83(3)
		M87D-TD11	17.916	18.45	0.534	2.064		0.92(3)
		M87D-TD12	18.81	20.175	1.365	2.424		1.08(3)
		M87D-TD13	20.53	21.07	0.54	2.779		1.24(3)
		M87D-TD14	21.075	23.17	2.095	2.784		1.24(3)
		M87D-TD15	23.18	26.309	3.129	2.794		1.24(3)

(*continued on next page*)

Table 1 (*continued*)

Basin	Hole	SBP-scale event	Top core depth (m)	Bottom core depth (m)	Thickness (m)	Event-free depth (m)	Age estimate (ka) based on (1) event-free sed. rate (Datum 1/2 to Datum 3); (2) estimated age of correlative tie-point (Table 2); (3) on margin-wide average event free sed. Rate (2.25 mm/yr)
Northern Japan Trench							
N1	M0086B	M86B-TD1	0	0.923	0.923	0	–
		M86B-TD2**	7.49	17.588	10.098	6.567	1.77
N2	M0088D	M88D-TD1**	1.888	14.812	12.924	1.888	1.77
		M88D-TD2	16.36	16.988	0.628	3.436	2.31(2)
		M88D-TD3	30.05	35.662	5.612	16.498	–
N3	M0084D	M84D-TD1**	3.185	18.355	15.17	3.185	1.77(2)
		M84D-TD2	19.845	20.515	0.67	4.675	2.31(2)
		M84D-TD3	29.985	32.015	2.03	14.145	5.76(2)
		M84D-TD4	33.9	35.18	1.28	16.03	6.21(2)
N3	M0085D	M85D-TD1**	1.398	2.321	0.923	1.398	1.77
		M85D-TD2	13.2	13.79	0.59	12.277	6.25(1)
		M85D-TD3	24.07	25.368	1.298	22.557	10.49(1)
		M85D-TD4	28.55	29.34	0.79	25.739	11.80(1)
		M85D-TD5	31.32	33.78	2.46	27.719	12.62(1)

NB: * = SBP-scale event beds correlated to the 869 CE Jogan earthquake. ** = SBP-scale event beds correlated to 1.77 ka bed.

in the trench-fill sequence. This can be explained by core-expansion that is caused by decompression of the cores as they are brought to the surface and further gas expansion and stretching during core handling process on deck (Strasser et al., 2023). We corrected for this by manually "recompressing" the density profile between two correlation tie-points to visually fit marker horizons in the SBP data.

3.4. Stratigraphic correlation

Stratigraphic correlation between Sites in the same basin (c.f. "composite stratigraphy approach", section 3.1) is based on a series of unique tie points (TP) defined by distinct lithology and physical property characteristics (listed in Table 2 according to Basin number). The majority of tie points are documented at the base of SBP-scale event deposits, since they demonstrate the clearly-defined spikes and overlying trends in MS, density and NGR data. In the uppermost part of the stratigraphic succession at Sites in the southern and central Japan Trench, this includes a tie point between a SBP-scale event bed that has been previously cored, dated and related to deposits from the 869 CE earthquake (see correlated beds in Figs. 4–9; Kioka et al., 2019a; McHugh et al., 2020; Schwestermann et al., 2020; Ikehara et al., *2016, 2017a*; Kanamatsu et al., *2022, 2023*; Bao et al., 2018). This defines the first inter-basin tie point (ITP1; Table 2) which is used to make initial correlations along the southern-central Japan Trench.

Since SBP-scale event beds mapped at depocenter Sites often pinch out to <0.5 m thick at basin edges, the equivalent horizons are not mapped as SBP-scale in the condensed sections cored at basin margin Sites. Thus, stratigraphic correlation between Sites in the same basin (and between basins) is not possible based on SBP-scale event beds alone. As a result, we also interrogate the stratigraphic sequences at each Site to the lithofacies level in order to resolve many more additional tie points. Shown as solid lines in Figs. 4, 5, 7, and 9, and listed in Table 2, these tie points are defined at horizons that demonstrate uniquely identifiable physical property trends and characteristically recurring patterns (e.g., distinct double peak in MS at ca. 13 mbsf in M0082D correlates to the base of M81D-TD8 along S1-TP4; Fig. 4; Figs.S1, S2). Several other more tentative correlations are noted as dashed lines in Figs. 4–7 and 9, but these require further analysis to confirm their equivalence.

Where possible, we also implement tie points from tephra marker beds identified by shipboard smear-slide-based volcanic glass and heavy mineral component analyses (Strasser et al., 2023). In some cases, tephra horizons with similar geochemical composition and stratigraphic position are identified between basins. We attribute these horizons as inter-basin tie points (ITP2, and − 3; Table 2; Figs. 4–7 and 9).

3.5. Event stratigraphy age constraints

In the southern and central Japan Trench, we use the correlated 869 CE Jogan event deposits (ITP1) as Datum 1 (1.081 ka (calendar years before present (1950 CE))). In the northern Japan Trench, Datum 2 (~1.77 ka) is defined by the U2-N08 event bed mapped in Basin N3 by Kioka et al. (2019a) and dated to 1.77 (+0.49/−0.31) ka by Usami et al. (2021) and Schwestermann et al. (2021). This event bed is equivalent to our M84D-TD1 in Basin N3 and can be correlated to the other northern basins along tie point ITP4 (see detailed description in section 4.2.4). In addition to these two datums, we obtain additional chronostratigraphic constraints from shipboard radiolarian biostratigraphy (Strasser et al., 2023), which should be considered tentative before confirmation by detailed post-expedition analyses. Therefore, we only consider data from cores that have high sampling resolution of >1 sample per 2 m, which includes M0092D, M0090D, M0089D, and M0085D. We utilize the age and depth of the boundary between *C. davisiana* zone a' and b', previously dated near the Holocene/late Pleistocene boundary at ca. 11 ka (Morley et al., 1982; Itaki et al., 2009). Hence, this forms Datum 3 (~11 ka) in cores M0092D, M0090D, M0089D, and M0085D, defined at the average depth of samples between which the sharp downward increase in relative abundance of *C. davisiana* (from <5 % above to >10 % below; defining the top of *C. davisiana* Zones b1) occurs (Table 3). Using this key datum, average event-free sedimentation rates (i.e., free of >0.50 m events) are calculated for the above-mentioned Holes using linear interpolation between Datum 1 (869 CE) or 2 (~1.77 ka) and Datum 3 (~11 ka) (Table 3). Considering these sedimentation rates, we can provide initial age estimates for SBP-scale event deposits and stratigraphic tie-points located between datums in Holes with biostratigraphic age constraints, which can then be correlated across to Holes without biostratigraphic information (Tables 1–2). For basins, where stratigraphic correlation is not possible, we offer more tentative age estimates using a margin-average event-free sedimentation rate of 2.25 mm/yr (constrained by the average event-free sedimentation rate calculated in the above-mentioned Holes; Tables 1–3). Since the biostratigraphic datums do not offer precise ages at a given depth, and sedimentation rates likely are not strictly linear throughout the Holocene, we do not provide age uncertainty ranges but consider the interpolated ages as only "reasonable" estimates, with uncertainties of up to ~700 years (as constrained by the range of age estimates for tie-points in different Holes and comparison to correlations to event deposits dated by precise paleomagnetic secular variation (PSV) stratigraphy by

Table 2
Tie points.

Tie-point	Hole	Core depth (m)	Event-free core depth (m)	Age estimate (ka) based on event-free sed. rate (Datum 1/2 to Datum 3)
Southern Japan Trench				
S1-TP1	M0081D	5.324	3.276	–
	M0082D	2.097	2.097	–
S1-TP2	M0081D	15.125	5.671	–
	M0082D	6.344	4.764	–
S1-TP3	M0081D	21.465	10.751	–
	M0082D	11.017	9.437	–
S1-TP4	M0081D	23.77	12.406	–
	M0082D	13.051	11.471	–
S1-TP5	M0081D	29.677	18.313	–
	M0082D	18.588	17.008	–
S1-TP6	M0081D	30.212	18.848	–
	M0082D	19.14	17.56	–
S1-TP7	M0082D	23.7996	22.2196	–
S2-TP1	M0095B	16.282	14.257	–
	M0092D	19.05	13.512	6.43
S2-TP2	M0095B	17.06	15.035	–
	M0092D	19.94	14.402	6.89
Central Japan Trench				
C1-TP1	M0090D	15.81	15.81	6.19
C2-TP1	M0083F	18.36	7.16	–
	M0089D	5.2	5.2	2.08
C2-TP2	M0083F	20.095	8.37	–
	M0089D	6.69	6.69	2.78
C2-TP3	M0083F	26.335	13.475	–
	M0089D	12.04	12.04	5.29
C2-TP4	M0083F	27.77	14.04	–
	M0089D	12.6	12.6	5.55
C2-TP5	M0083F	30.25	16.52	–
	M0089D	14.54	14.54	6.47
Central/Northern Japan Trench				
No robust tie points at boundary area between central/northern Japan Trench				
Northern Japan Trench				
N3-TP1	M0084D	21.4	5.56	–
	M0085D	3.64	2.717	2.31
N3-TP2	M0084D	32.015	14.145	–
	M0085D	12	11.077	5.76
N3-TP3	M0084D	33.73	15.86	–
	M0085D	13.08	12.157	6.21
Inter-basin tie points (ITP)				
ITP1	M0081D	12.888	5.279	1081 (869 CE)
	M0082D	5.03	3.45	1081 (869 CE)
	M0095B	6.409	4.3841	1081 (869 CE)
	M0092D	8.709	3.171	1081 (869 CE)
	M0091D	13.184	6.8127	1081 (869 CE)
	M0090D	3.197	3.197	1081 (869 CE)
	M0089D	3.07	3.07	1081 (869 CE)
	M0083F	15.44	4.24	1081 (869 CE)
ITP2	M0090D	25.75	25.75	10.21
	M0089D	23.095	23.095	10.48
ITP3	M0087D	20.175	2.424	–
	M0094B	15.117	2.605	–
ITP4	M0086B	17.588	6.567	1.77
	M0088D	14.812	1.888	1.77
	M0084D	18.355	3.185	1.77
	M0085D	2.321	1.398	1.77

Kanamatsu et al., 2023; see details in section 4 and discussion in section 5). Despite the large uncertainties, this first-order estimates are considered appropriate for testing the SBP-based event predictions of Kioka et al. (2019a).

Given the goal of the study is to examine the prehistoric event sequences for paleoseismology applications, we do not attempt to constrain event ages above the Datum 1 (869 CE). Instead, we rely on the good agreement between our observed SBP-scale events beds and the previously published documentation of deposits in the uppermost trench-fill sequences to make any inferences regarding historical earthquakes. Similarly, we do not provide age estimates for SBP-scale event deposits that occur stratigraphically before the oldest Datum 3 (~11 ka). Ongoing studies aim to provide more thorough age control for the full sequences captured by the IODP Exp. 386 cores using more precise dating techniques which should allow the synchronicity criterion for seismic-triggering to be more accurately assessed. Until then, we use the age estimates derived in this study to conceptually discuss potential of the new event stratigraphy results for interpreting submarine paleoseismology Japan Trench.

4. Results

4.1. Event deposit characterization

A total of 77 SBP-scale (>50 cm thick) event deposits are identified in the studied holes (Supplementary Figs. S1-S15; Table 1). Most deposits are characterized by (1) a fining-upward sequence from a sharp, erosional basal surface below (2) a typically few cm to occasionally dm

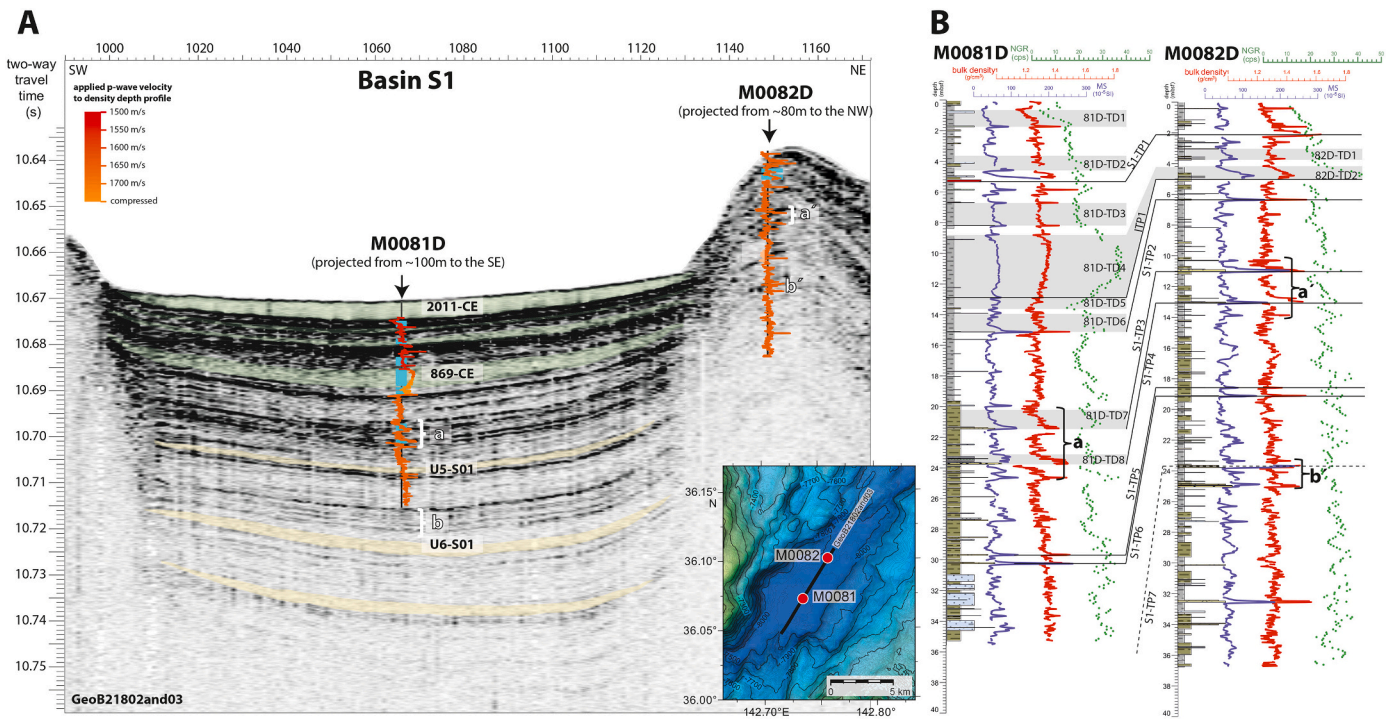

Fig. 4. SBP-scale event deposits imaged and sampled in Basin S1 of the Southern Japan Trench (see Fig. 2 for location). (A) SBP profile from Kioka et al. (2019a), with depth-to-TWT converted density profiles of Holes M0081D and M0082D. Different colours of the density profiles give approximated p-wave velocities applied for the depth conversion. Intervals in teal colour mark SBP-scale even deposit (this study). SBP units shaded in green were previously cored, validated and dated. SBP units in yellow were interpreted by Kioka et al. (2019a) but not validated previously. (B) Lithology, MS, density, and NGR logs of M0081D and M0082D, with SBP-scale event deposits (shaded in grey) and tie-points correlating event deposits and marker horizons between the sites. For letter annotations a, a′, b, b′, see text for detailed descriptions. For legend of symbols used in the lithostratigraphic columns see Supplementary Fig. S16. (For interpretation of the references to colour in this figure legend, the reader is referred to the web version of this article.)

thick coarser (sandier) bed with high MSCL density values, grading through (cross-)laminated and/or graded sand to (3) a fine-grained interval that generally lacks any sedimentary structures or bioturbation, varies in thickness from a few decimetres to up to several meters has variable MSCL bulk-density values depending on different decompaction and degassing processes during core recovery Fig.3a-d). Gradual, upward-decreasing trends in MS and NGR often indicate that these fine-grained intervals are also normally graded. These observations indicate that following the deposition of the coarser base by waning turbidity currents, suspension settling of large-amounts of remobilized fine-grained sediment particles is the dominant depositional process and focuses thicker deposition in the depocenter of the trench-fill basins. Several event deposits show characteristic MS and NGR signals but in places with a slightly different pattern e.g., basal peaks may either be both positive or show opposite trends, indicating that the distribution of magnetic minerals and/or radioactive elements in the event deposits is not solely controlled by grain size but may be indicative for the sediment provenance.

The thickest event deposits are reported in the northern Japan Trench Sites M0086, M0088 and M0084 (10.1, 12,9 and 15.2 m thick respectively). The lower parts of the thickest fine-grained intervals have soft-sediment deformation structures such as contorted and dipping beds, recumbent and isoclinal folds, and floating silt and sand patches, suggesting deposition from likely fluidized flows with plastic rheology (Fig. 3e, g, h). These intervals show significantly reduced bulk density values (<1.4 g/cm^3) and are hypothesized to have experienced significant degassing during core recovery (Strasser et al., 2023).

At boundary area between the central and northern Japan Trench, the cored sequence at Site M0094 and M0087 is composed of 82 % and 89 % superimposed thick event deposits, with only thin intervals between event deposits that have signatures of bioturbation. Here, event deposits comprising matrix (clay)-supported mud clasts with subrounded and irregular shapes are suggested to document debris flow deposition from potentially local submarine landslides processes. This type of event deposit is not observed in trench basins elsewhere along Japan Trench, except for a similar occurrence at the bottom of Hole M0085D.

4.2. Correlation and dating of event deposits

In the following section, we present event stratigraphic interpretation and correlation initially focused on four basins that are representative of sequences at the southern, central, and northern Japan Trench, and the boundary area between the central and the northern Japan Trench (Figs. 4–7). Core-SBP correlation for all other basins are presented in Fig. 8 and full event-stratigraphy correlation along the entire trench is presented in Fig. 9.

4.2.1. Southern Japan Trench

The depocenter of the southernmost Basin S1 has an area of ~29.4 km^2 and is located at the greatest water depth of more than 8000 mbsl. The basin has a comparably large catchment area (flow accumulation area ~ 1.36 × 10^{10} m^2; Kioka et al., 2019a; Supplementary Table (Tab—S1)). Here, the stratigraphic succession at Site M0081D contains 8 SBP-scale event beds (M81D-TD1 to -TD8), comprising 32 % of the cored stratigraphic succession. The condensed section cored at Site M0082D at the margin of the same basin only contains two SBP-scale event beds (M82D-TD1, -TD2), representing only 4 % of the cored sequence.

Core-to-SBP correlation in the upper 10 m of the basin depocenter at Site M0081 generally reproduces the event sequences previously documented within dated core GeoB21804 (at basically same location as Site

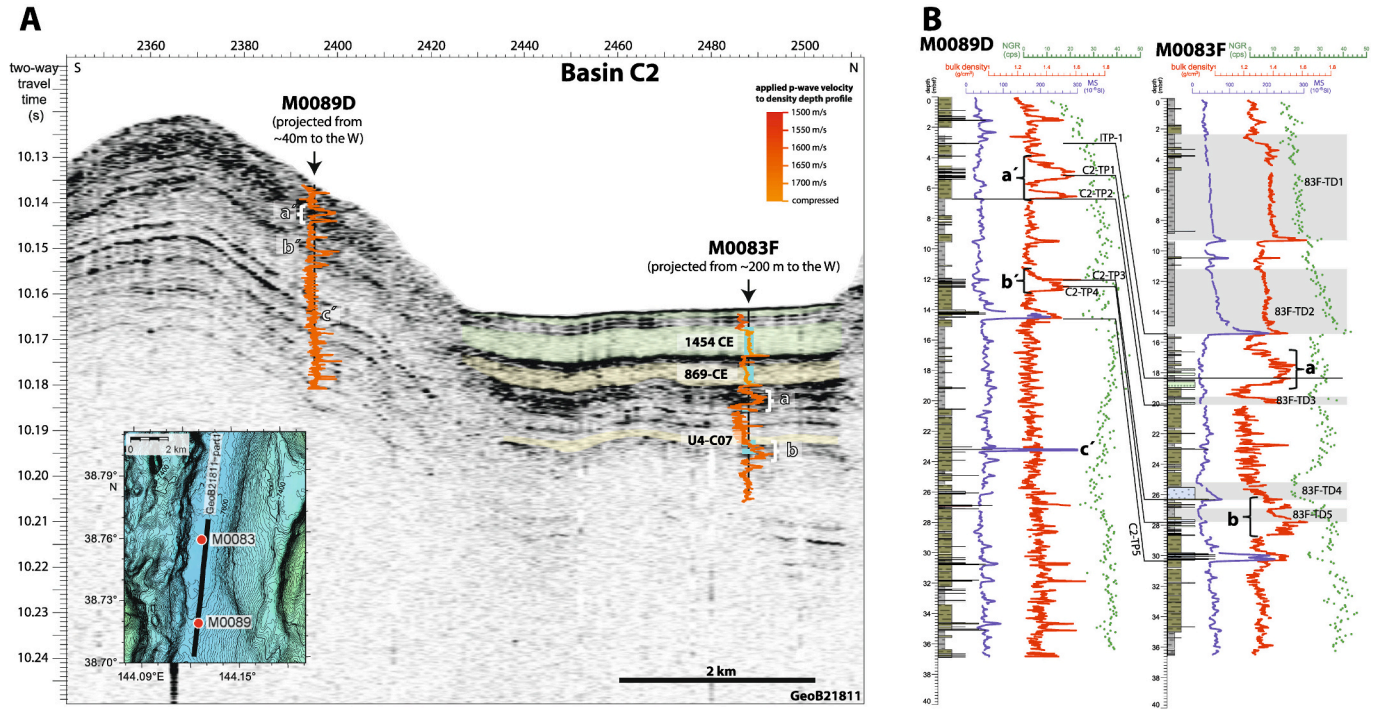

Fig. 5. SBP-scale event deposits imaged and sampled in Basin C2 of the Central Japan Trench (see Fig. 2 for location). (A) SBP profile from Kioka et al. (2019a), with depth-to-TWT converted density profiles of Holes M0083F and M0089D. Different colours of the density profiles give approximated p-wave velocities applied for the depth conversion. Intervals in teal colour mark SBP-scale even deposit (this study). SBP units shaded in green were previously cored, validated and dated. SBP units in yellow were interpreted by Kioka et al. (2019a) but not validated previously. (B) Lithology, MS, density, and NGR logs of M0083F and M0089D, with SBP-scale event deposits (shaded in grey) and tie-points correlating event deposits and marker horizons between the sites. For letter annotations a, a′, b, b′, see text for detailed descriptions. For legend of symbols used in the lithostratigraphic columns see Supplementary Fig. S16. (For interpretation of the references to colour in this figure legend, the reader is referred to the web version of this article.)

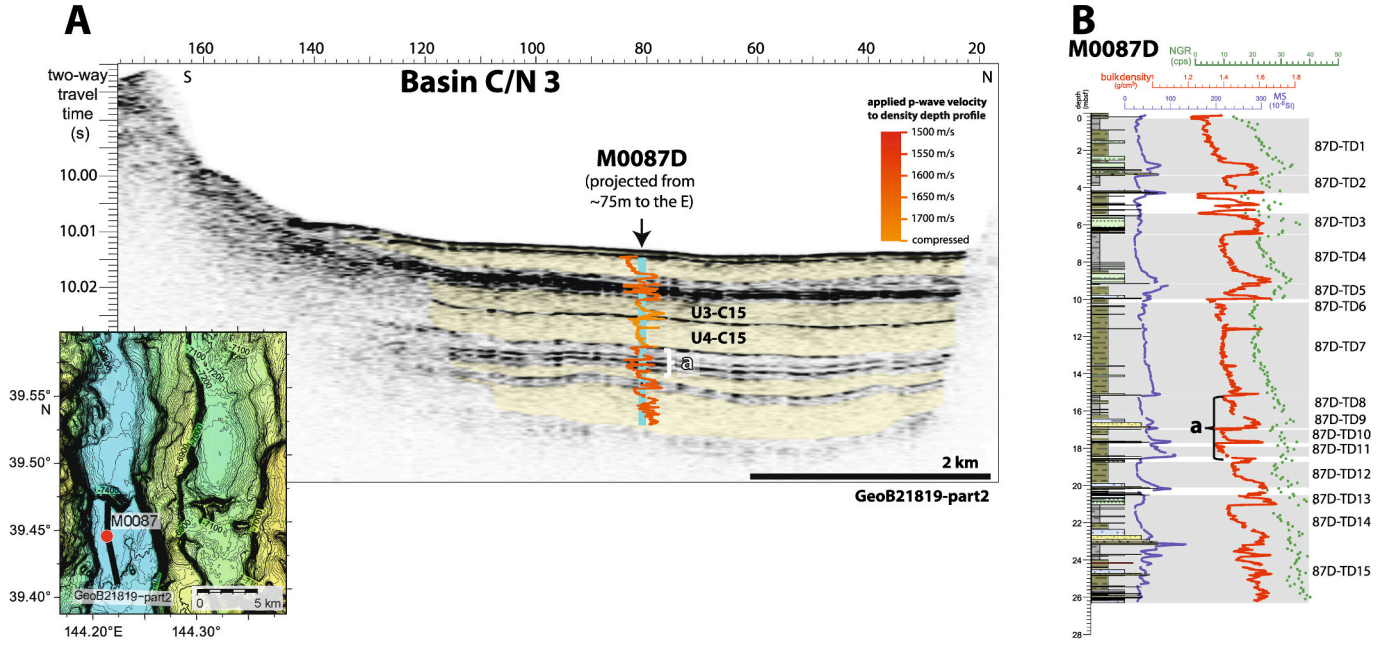

Fig. 6. SBP-scale event deposits imaged and sampled in Basin C/N3 of the "Boundary Area" between the Central and Northern Japan Trench (see Fig. 2 for location). (A) SBP profile from Kioka et al. (2019a), with depth-to-TWT converted density profiles of Holes M0083F and M0089D. Different colours of the density profiles give approximated p-wave velocities applied for the depth conversion. Intervals in teal colour mark SBP-scale even deposit (this study). SBP units shaded in yellow indicated that they were interpreted by Kioka et al. (2019a) but not yet previously validated by coring (B) Lithology, MS, density, and NGR logs of M0087D SBP-scale event deposits (shaded in grey) For letter annotations a see text for detailed description. For legend of symbols used in the lithostratigraphic columns see Supplementary Fig. S16. (For interpretation of the references to colour in this figure legend, the reader is referred to the web version of this article.)

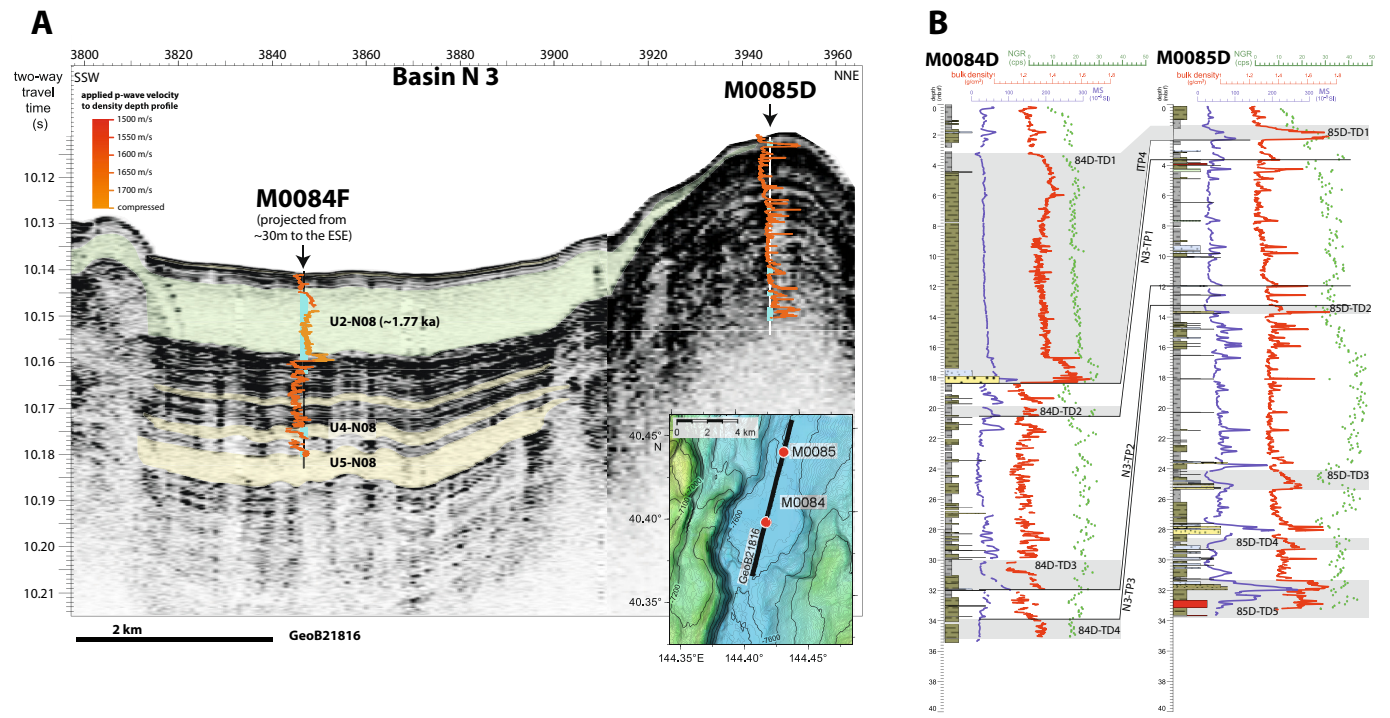

Fig. 7. SBP-scale event deposits imaged and sampled in Basin N3 of the Northern Japan Trench (see Fig. 2 for location). (A) SBP profile from Kioka et al. (2019a), with depth-to-TWT converted density profiles of Holes M0084D and M0085D. Different colours of the density profiles give approximated p-wave velocities applied for the depth conversion. Intervals in teal colour mark SBP-scale even deposit (this study). SBP units shaded in green were previously cored, validated and dated. SBP units in yellow were interpreted by Kioka et al. (2019a) but not validated previously. (B) Lithology, MS, density, and NGR logs of M0084D and M0085D, with SBP-scale event deposits (shaded in grey) and tie-points correlating event deposits and marker horizons between the sites. For legend of symbols used in the lithostratigraphic columns see Supplementary Fig. S16. (For interpretation of the references to colour in this figure legend, the reader is referred to the web version of this article.)

M0081; Kioka et al., 2019a; McHugh et al., 2020), revealing that 81D-TD4 corresponds to the 869 CE Jogan event deposits (Fig. 4). The >2 m-thick structureless clay interval of 81D-TD4 exhibits very high NGR values (>35 cps), defining a characteristic marker that can be correlated across all sites in the southern and central Japan Trench (ITP1; Fig. 9; Table 2). Hence, we also identify M82D-TD2, with its equally distinct high NGR signal and facies association to be the correlative 869 CE Jogan event in M0082D. This correlation is further confirmed by the common stratigraphic position of M82D-TD2 between a tephra layer (S1-TP1) and a prominent marker horizon characterized high MS, density and NGR values (S1-TP2).

Below the S1-TP2 tie point in M0081D, the interval comprising M81-TD7 and M81-TD8 corresponds to four high-amplitude horizons with only thin intercalated acoustically-transparent bodies in SBP-data. These SBP-scale event beds (labelled a in Fig. 4) were not previously identified by Kioka et al. (2019a). The correlative interval at Site M0082 (labelled a´ in Fig.4) shows two high-amplitude horizons in SBP data that correspond to two events beds of <50 cm thickness but with distinct fining-upward successions, basal graded sand beds with elevated MS, density and NGR values (S1-TP3 and S1-TP4).

Similarly, two deeper events beds with typical turbidite facies succession but thickness < 50 cm are correlated across S1-TP5 and S1-TP6 in M0081D (ca. 30 mbsf) and M0082D (ca. 19 mbsf) (Fig. 4). These horizons correspond to two distinct high-amplitude horizons in the SBP data (Fig. 4). S1-TP5 correlates with the base of event bed 'U5-S01' identified in SBP data by Kioka et al. (2019a).

In the deeper stratigraphic succession, no further clear tie point to correlate between M0081D and M0082D is identified. However, the upper part of a 2 m thick succession at the basin margin Site M0082 (ca. 23.5–25 mbsf; characterized by several <0.5 m event deposits with prominent MS and density peaks, but comparably lower NGR values; labelled b' in Fig.4), is likely equivalent to an event-bed succession imaged below the base of Hole M0081D in SBP data by high-amplitude reflections intercalated with thin acoustically-transparent bodies (labelled b in Fig.4). Given the significantly thicker event deposit sequence at the depocenter Site, the thick event bed mapped as 'U6-S01' by Kioka et al. (2019a) could roughly correlate with S1-TP7.

For the other investigated trench basins of the Southern Japan Trench, there also is generally good agreement between the sequence of event deposits predicted from the SBP data by Kioka et al. (2019a) and the occurrence of SBP-scale event deposits in the IODP Expedition 386 cores (Fig. 8). The base of the previously identified 869 CE event bed (Kioka et al., 2019a; McHugh et al., 2020; Schwestermann et al., 2020; Ikehara et al., *2016, 2017a*; Kanamatsu et al., *2022, 2023*; Bao et al., 2018) shows highest NGR values throughout, defining a stratigraphic marker that correlates M82-TD2, M95B-TD2, M92D-TD4, M91D-TD3 to M83F-TD2 (ITP1; Fig. 9). We acknowledge that this correlation currently only considers SBP-scale event deposits and does not examine along-strike facies variations, nor detailed facies analyses of overlying sequences comprising thinner beds that may or may not also be related to the 896 CE event sequence (see discussion in section 5).

There are no SBP-scale event deposits identified below ITP1 in Basin S2, which has comparably smaller size and catchment areas (< 4 km^2 basin size and < 10^{10} m^2 flow accumulation area) compared to Basins S1 and S3 (Fig. 2a; Table S1). Below ITP1 in Basin S2, a sequence of prominent high amplitude reflections in SBP data (labelled a in Fig. 8) correspond to two distinct sand beds with unique physical properties in Hole M0095B and M0092D (Fig. 9). In both Holes, the upper sand bed (S2-TP1) has particularly high MS values, and the lower sand bed (S2-TP2) has particularly low NGR values (Fig. 9). The equivalent pattern is recognised at 23,5- 25mbsf in M0082D. Thus, we infer tentative correlation between S2-TP1 and S1-T7. The roughly estimated ages of tie-points S2-TP1 and S2-TP2 are ~6.4 ka and ~ 6.9 ka, as calculated from average sedimentation rate between Datums 1 and 3 in Hole

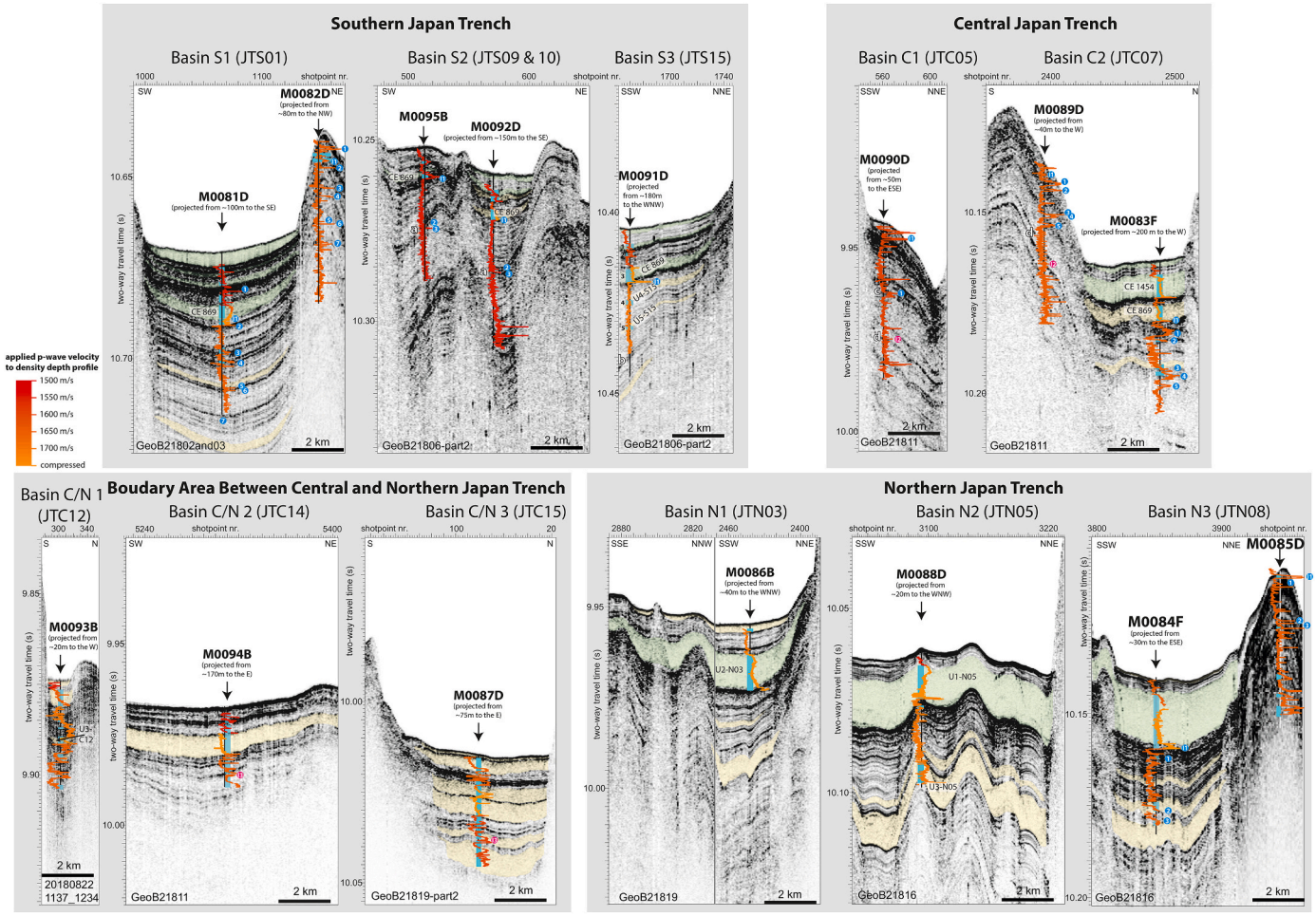

Fig. 8. Core-to-SBP correlation for all basins sampled by IODP Expedition 386 GPC operations (see Fig. 2 for locations). SBP profiles are from Kioka et al. (2019a). SBP units shaded in green were previously cored, validated and dated. SBP units in yellow were interpreted but not validated previously. Depth-to-TWT converted density profiles of the deepest holes cored at each site are shown to illustrate the correlation between the cores (with density as proxy for impedance) and SBP reflection data. Different colours of the density profiles give approximated p-wave velocities applied for the depth conversion. SBP-scale deposits identified in cores are shown by teal squares behind the density profiles. Blue circles are tie-points (with the respective tie-point annotation per site indicated by the single number). For letter annotations a, b, c, and d see text for detailed descriptions. (For interpretation of the references to colour in this figure legend, the reader is referred to the web version of this article.)

M0092D (Tables 2,3). The same characteristic sequence comprising event deposits below SBP scale showing prominent MS and density peaks, but low NGR values with a roughly similar estimated age also occurs in Basins C1 and C2 and correlation is inferred between S2-TP2 (~6.9 ka), C1-TP1 (~6.2 ka) and C2-TP5 (~6.5 ka) (Fig. 9; see more details in 4.2.2 and further discussion in 5.3).

Flow accumulation is highest in Basin S3 (source area of ~2.2 × 10^{10} m^2; basin size 8.2 km^2). In Hole M0091D, 28 % of the cored stratigraphic sequence is built by 5 SBP-scale event deposits (M91D-TD1 to -TD5; Fig. 9). SBP-scale event deposits M91D-TD3 to -TD5 correspond to the acoustically transparent bodies U3-S15, U4-S15, and U5-S15 mapped in Basin S3 by *Kioka* et al. (2019a; Fig. 8). M91D-TD3 is correlated to the 869 CE event deposit (ITP1), but no unique inter-basin correlation can be identified for M91D-TD4 and -TD5. SBP-to-core correlation reveals that the base of Hole M0091D did not reach the underlying high-amplitude reflections (labelled b in Fig. 8) which indicate an interval likely comprised of several event beds. Such an interval probably correlates to the above described 6.2–6.9 ka sequences in Basin S2 (S2-TP2; labelled a in Fig. 8) and Basin C1 (C1-TP1; labelled c in Fig. 8).

4.2.2. *Central Japan Trench*

Basin C2 has size of ~4 km^2 and the largest flow accumulation area in the central Japan Trench (~ 1.2 × 10^{10} m^2; Kioka et al., 2019a). At Site M0083, 37.5 % of the cored stratigraphic succession is built by 5 SBP-scale event deposits (M83F-TD1 to M083F-TD5), while the condensed basin margin section at Site M0089 only comprises event deposits <50 cm thickness (Fig. 5). Average background sedimentation rates in Basin C2 (as calculated for event-free thickness in Hole M0089D) are 2.1 mm/yr between Datum 1 (869 CE) and Datum 3 (~11 ka).

Core-to-SBP correlation at Site M0083 clearly links the upper two SBP-scale event deposits, M83F-TD1 and -TD2, to the acoustically transparent bodies U2-C07 (1454 CE Kyotoku event) and U3-C07 (869 CE Jogan event) mapped in SBP data by *Kioka* et al. (2019a; Fig. 5). Below these SBP-scale deposits at Site M0083, the interval between 16.5 and 18.75 mbsf contains several few-cm to up-to-20 cm thick event beds with parallel-laminated very fine sand, sandy silts and silt exhibiting high density but MS values that are remarkedly weaker than those of overlying and underlying hemipelagic intervals (Supplementary Fig. S3). This facies with such remarkedly low magnetic susceptibility is characteristic for the previously identified ~2.3 ka event sequences, which was described, precisely dated (by means of paleomagnetic secular variation (PSV) stratigraphy) and correlated across several basins in the central Japan (Kanamatsu et al., 2023). In Basin C2, this sequence correlates to the upper part of a thick (0.5 ms TWT) interval in SBP data characterized by closely-spaced high-amplitude reflections (labelled a in Fig. 5). The lower part of this SBP-interval includes a thin,

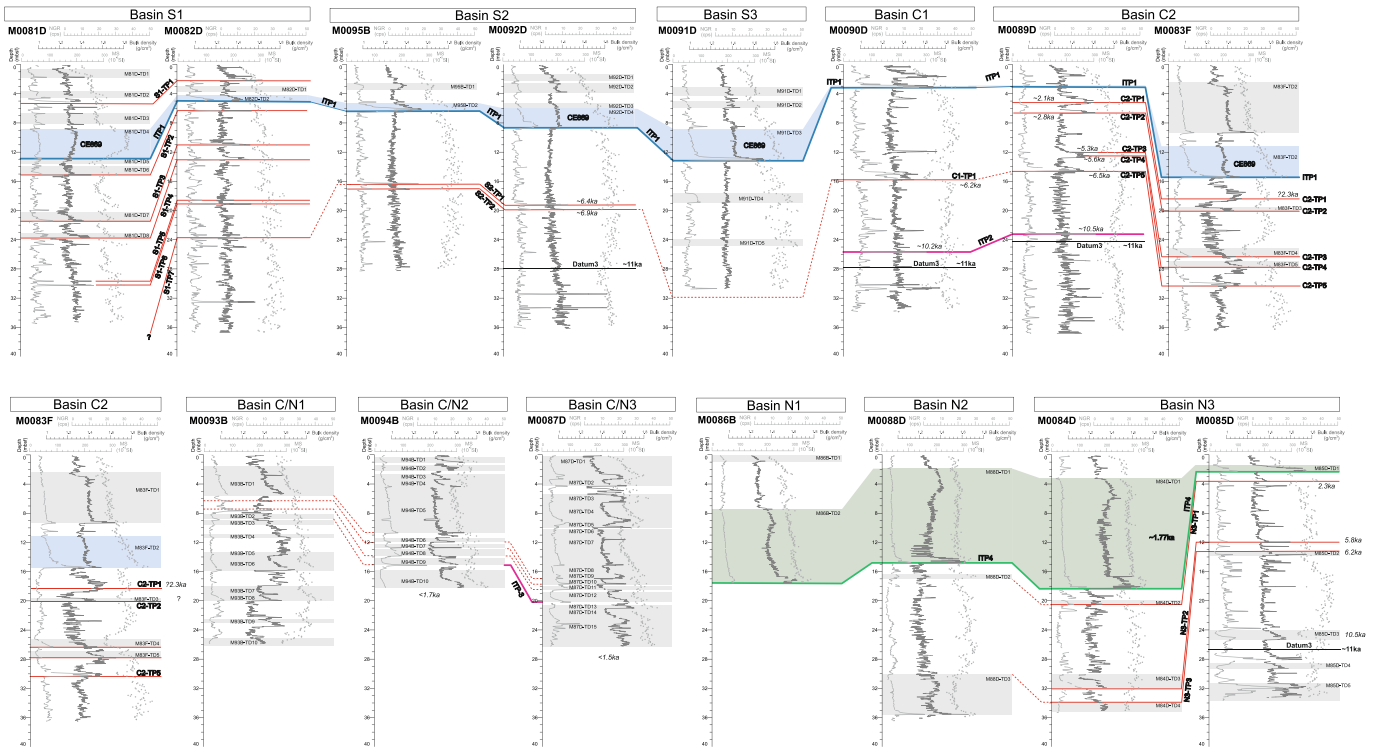

Fig. 9. Stratigraphic correlation of SBP-scale event deposits and stratigraphic markers beds (Tie-points; TP) across the entire Japan Trench. See Fig. 2 for locations of sites. Background data are MS, density and NGR for the deepest Hole cored at each site. SBP-scale event deposits are coloured as follows: blue = 869 CE event deposits that were previously cored, dated and validated to correlate with the historic Jogan earthquake and tsunami. Interbasin correlation is confirmed in this study by correlation along interbasin tie-point ITP1 (blue solid line), here used as Datum 1 (1081 ka). Green = ~1.77 ka event deposits in the northern Japan Trench the upper part of which was previously cored and dated by Usami et al. (2021) and Schwestermann et al. (2021). Interbasin correlation is confirmed in this study by correlation along interbasin tie-point ITP4 (green solid line), here used as Datum 2 (~1.77 ka). The two other interbasin tie-points based tephra beds described in Strasser et al. (2023) here used as ITP2 and ITP3 are shown be pink solid lines between basins C1 an C2, and between basins C/N 2 and C/N3. Tie-points correlating SBP-scale event deposits or unique thinner marker beds between two Sites in the same basin are shown as solid red lines. Where interbasin correlation between such marker beds is inferred, we indicate possible correlation between basins by a dashed red line. The average-depth position of the interval within which Datum 3 (~11 ka) was identified by shipboard radiolarian biostratigraphy in Holes M0092D, —90D, —89D and 85D (Strasser et al., 2023) is indicated by a solid black line. Estimated ages of marker bed discussed in the text are indicated in cursive black (uncertainties of these age estimated may be as large as ~700 kyrs.) (For interpretation of the references to colour in this figure legend, the reader is referred to the web version of this article.)

laterally-variable acoustically-transparent body that corresponds to M83F-TD3 (base represents C2-TP2), but was not previously identified as event deposit by Kioka et al. *(2019a)*. The same characteristic stratigraphic succession and physical property (particularly low MS) pattern is identified at Site M0089 (between ~4.1 and ~ 6.5 mbsf in Hole D; correlated along C2-TP1 and C2-TP2), where SBP data also shows high-amplitude reflections (labelled a´ in Fig. 5). By calculating event-free sedimentation rate between Datum 1 (869 CE) and Datum 3 (~11 ka) in Hole M0089D, the ages of C2-TP1 and C2-TP2 (thus M83F-TD3 also) are estimated to be ~2.1 ka and ~ 2.8 ka, respectively. This supports possible correlation between the low-MS turbidite event sequence with the ~2.3 ka event by Kanamatsu et al. (2023), considering our age estimates derived from average sedimentation rates have uncertainty of several hundreds of years (see discussion in section 5).

High-amplitude reflections at ~15 ms TWT-depth at Site M0089 (labelled b´ in Fig. 5) result from a 75 cm-thick succession including thin interbedded silty-sand deposits with pronounced density peaks and variable MS/NGR signals (Fig. 5). We correlate M0089D and M0083F below this interval via C2-TP3 (prominent MS/density peaks with comparably low NGR) and C2-TP4 (low MS but comparably high NGR values). These tie points correlate with the base of SBP-scale deposits 83F-TD4 and 83F-TD5 at Site M0083, which link to acoustically-transparent bodies between high-amplitude reflections (labelled b in Fig. 5). The upper body corresponding to 83F-TD4 was previously mapped as U4-C07 by Kioka et al. (2019a). By calculating event-free sedimentation rate between Datum 1 (869 CE) and Datum 3 (~11 ka) in Hole M0089D, we estimate the age of C2-TP3 (and 83F-TD4) to be 5.3 ka and C2-TP4 (and 83F-TD5) to be 5.6 ka.

Further correlation between Site M0083 and Site M0089 is possible along tie point C2-TP5 (~6.5 ka), which is defined at the sharp base of a ~ 40 cm sequence with pronounced double peaks in MS/density and low NGR values (Supplementary Fig. S8). The same characteristic sequence comprising event deposits below SBP scale showing prominent MS and density peaks, but low NGR values also occurs at similar stratigraphic depth in Basin C1 (Fig. 9; base represents C1-TP1; ~6.2 ka), where the thicker sequence (> 1 m) also corresponds to high-amplitude horizons (labelled c in Fig. 8). Considering such multiple evidence for stratigraphic correlation and acknowledging significant uncertainties of several hundreds of years for our rough age estimates, we infer that tie points C2-TP5 and C1-TP1 can be used to link equivalent stratigraphic sequences between basins in the central Japan Trench, and potentially even further to the south if C1-TP1 also correlates with S2-TP2 (~6.9 ka) and the event bed immediately below S1-TP7 (~ 6.4 ka) (Fig. 9; see 4.2.1 and discussion in Section 5.2).

The lower part of the cored succession in Basin C1 and C2 can be linked along ITP2, which is defined by a characteristic tephra layer composed of pumiceous type volcanic glass, abundant hornblende (including hornblende-similar cummingtonite) and characteristic ß-quartz (Strasser et al., 2023; Table 2). Shipboard analyses did not yet allow conclusive correlation of this tephra to a dated volcanic eruption on land. Rough age estimates based on average sedimentation rates between Datums 1 and 3 are 10.2 and 10.5 ka in Holes M0090D and

Table 3
Sedimentation rates.

Basin	Hole	Total hole depth (m)	Total event thickness (m)	Total event-free thickness (m)	Percentage event thickness (%)	Datum 1 (869 CE)		Datum 2 (1770 CE)		Datum 3 (11 ka biostrat.)		Sedimentation rate for Datum 1–3 (869CE to 11 ka)		Sedimentation rate for Datum 2–3 (1.77 ka to 11 ka)	
						Core depth of Datum 1	Event-free depth of Datum 1	Core depth of Datum 2	Event-free depth of Datum 2	Core depth of Datum 3	Event-free depth of datum 3	Event-free thickness between	Sed.rate between datums (mm/yr)	Event-free thickness between	Sed.rate between datums (mm/yr)
Southern Japan Trench															
S1	M0081D	35.57	11.364	24.206	31.95	12.888	9.372	–	–	–	–	–	–	–	–
S1	M0082D	36.67	1.58	35.09	4.31	5.03	4.31	–	–	–	–	–	–	–	–
S2	M0095B	38.345	2.0249	36.3201	5.28	6.409	4.3841	–	–	–	–	–	–	–	–
S2	M0092D	36.205	5.538	30.667	15.30	8.709	3.171	–	–	27.9	22.362	19.191	1.93	–	–
S3	M0091D	31.12	8.6683	22.4517	27.85	13.184	6.8127	–	–	–	–	–	–	–	–
Central Japan Trench															
C1	M0090D	33.935	0	33.935	0.00	3.2	3.2	–	–	27.7	27.7	24.5	2.47	–	–
C2	M0089D	36.9	0	36.9	0.00	3.07	3.07	–	–	24.2	24.2	21.13	2.13	–	–
C2	M0083F	36.605	13.73	22.875	37.51	15.44	4.24	–	–	–	–	–	–	–	–
Central/Northern Japan Trench															
C/N1	M0093B	26.135	11.676	14.459	44.68	–	–	–	–	–	–	–	–	–	–
C/N2	M0094B	18.28	14.916	3.364	81.60	–	–	–	–	–	–	–	–	–	–
C/N3	M0087D	26.345	23.515	2.83	89.26	–	–	–	–	–	–	–	–	–	–
Northern Japan Trench															
N1	M0086B	18.24	11.021	7.219	60.42	–	–	17.588	6.567	–	–	–	–	–	–
N2	M0088D	36.48	19.164	17.316	52.53	–	–	14.812	1.888	–	–	–	–		
N3	M0084D	35.44	19.15	16.29	54.03	–	–	18.355	3.185	–	–	–	–		
N3	M0085D	33.69	6.061	27.629	17.99	–	–	2.321	1.398	26.6	23.789	–	–	22.391	2.43

M0089D, respectively. However, the tephra corresponds to a prominent high amplitude reflection in both basins (labelled c and d in Figs. 5 and 8, respectively), thus revealing an opportunity to spatially map this important marker horizon across basins that are imaged by SBP data but have not yet been cored.

4.2.3. Boundary area between central and northern Japan Trench

Flow accumulation rates are in the order of 10^7 to 10^9 m^2 at the boundary area between the central and northern Japan Trench. The basin sizes range between 1 and 24 km^2 and the infill sequence is predominately composed of superimposed SBP-scale event deposits, with only thin intervals with signatures of bioturbation between (Fig. 9). At Sites M0094 and M0087, 10 and 15 SBP-scale deposits build 82 and 89 % of the cored stratigraphic succession, with only 2.3 m and 2.4 m of event-free sediment, respectively (Supplementary Figs. S11–12). A characteristic tephra layer (ITP3; Table 2) is reported in the lowermost part of Holes M0094B and M0087D (Fig. 9). The tephra layer is composed of pumiceous type volcanic glass with fewer fibrous type shards and abundant hornblende with a smaller amount of orthopyroxene and clinopyroxene (Strasser et al., 2023). Shipboard analyses did not yet allow conclusive correlation of this tephra to a dated volcanic eruption on land. Also, no biostratigraphic datums were identified so there are currently no direct age constraints available for any sites in the boundary area. If we consider the range of event-free sedimentation rate estimated at other Sites along the margin (1.9–2.5 mm/year; Table 3), the depositional ages of SBP-scale deposits at the bottom of Holes M0094B and M0087D likely are not much older than 1.7 and 1.5 ka, respectively, whereas the bottom of Hole M0093B likely is much older.

At Site M0087, core-to-SBP correlation clearly links SBP-scale event deposits in the core to acoustically transparent bodies in SBP data (Fig. 5). The higher resolution observations from the core reveal that some seemingly single acoustically transparent bodies in SBP are composed of superimposed sequences that each can be thicker than 50 cm. For instance, stacked M87D-TD4 and M87D-TD5 together comprise the SBP-body mapped as U3-C15 by Kioka et al. *(2019a)*. The base of this stacked unit, M87D-TD5 is characterized by an 80 cm thick sequence containing matrix (clay)-supported mud clasts akin to a "debris flow"-type deposit that is not well resolved in SBP data (Supplementary Fig. S12). Overlying this is M87D-TD4, which is characterized by a fining-upward sequence of sand-to-silt to structureless clay resulting from waning turbulent flow and settling of a large suspension cloud (Supplementary Fig. S7). Below this, the acoustically-transparent body mapped as U4-C15 by Kioka et al. (2019a) links to both M87D-TD7 and M87D-TD6, representing another example of multiple stacked depositional sequences depicted as a single event unit in SBP data (Fig. 6).

SBP-scale deposits M87D-TD9 to M87D-TD11 (16.23–18.45 mbsf) are interbedded with thin (<20 cm thick) bioturbated intervals and range in thickness between 50 and 100 cm. They have opposing stratigraphic trends in average bulk density (increasing upwards) and MS/NGR (average value per event decreasing upwards) and link to an interval between ~17–20 SBP-TWT depth, where Kioka et al. *(2019a)* did not map the subtle acoustically-transparent intervals between high-amplitude horizons (marked a in Fig. 5). Below this interval, M87D-TD12 immediately overlies ITP3 which links M94B-TD9 to 87D-TD12 (see circled I2 in Fig. 8).

Based on comparable facies successions and physical property patterns, we propose tentative correlation of M87D-TD9 to M94B-TD6, M87D-TD10 to M94B-TD6, and M87D-TD11 to M94B-TD8 (dashes lines; Fig. 9). The 4.34-m thick M87-TD7 may also correlate to M94B-TD5. The correlative event bed to M87-TD8 is smaller than <50 cm thick in M0094B. We also consider potential correlation of M94B-TD5 to M93B-TD1, with its underlying sequence between 6 and 8 mbsf showing similarly high MS values and upward increasing density trends, but in detail not identical event-deposit and facies sequences.

No clear correlation tie point can yet be identified in M0093B that links between Basin C2 and C/N1. However, we note that the interval between ~9.5 and 13.5 mbsf (between M93B-TD3 and M93B-TD5) is a 4 m-thick interbedded sequence without bioturbated intervals but composed of several thinner (3-15 cm thick) event beds with parallel-laminated very fine sand, sandy silts and silt exhibiting high density but remarkedly low MS values (Supplementary Fig. S13). This sequence shows mostly high-amplitude densely-spaced reflections in SBP data. It is overlying the acoustically-transparent body with lateral pinch-out geometries (U3-C12 mapped by Kioka et al., 2019a; Fig. 8) that links to M93B-TD6. Despite being 5 times thicker, this interval has comparable acoustic (densely spaced high-amplitude reflections) and sedimentary facies (interbedded parallel-laminated sands) and physical property characteristics (high density, remarkedly low MS) as the interval below the 869 CE event deposits in Basin C2, including C2-TP1, possibly correlative to the 2.3 ka event previously described by Kanamatsu et al. (2023) (see section 5.2 for discussion).

4.2.4. Northern Japan Trench

Flow accumulation along the entire Japan Trench is highest in the northernmost Basin N3 (ca. 5×10^{10} m^2; Fig. 2; basin size ~26 km^2 (Supplementary Table (Tab—S1))). Here, the largest acoustically-transparent body in all SBP data of the entire Japan Trench was identified at Site M0084 (U2-N08 mapped by *Kioka* et al.,2019a). In Hole M0084D, 54 % of the cored stratigraphic succession is built by 4 SBP-scale event deposits, the thickest of which is 15.17 m (M84D-TD1). At the margin of Basin N3, the stratigraphically-correlative but condensed section cored at Site M0085 is built by five thinner (<2.46-m-thick) SBP-scale event beds (M85D-TD1 to M085-TD5; Table 1). Overall, SBP-scale event deposits comprise 18 % of the entire cored sequence in Hole M0085D but only the top 2.46 m of mud (matrix)-supported pebbles and cobble clasts from M84D-TD5 was recovered. Average background sedimentation rates in Basin N3 (as calculated for event-free thickness in Hole M0085D; Table 3) are 2.4 mm/yr between Datum 2 (~1.77 ka) and 3 (~11 ka).

At Site M0084, core-to-SBP correlation clearly links event deposits M84-TD1, M84-TD3 and M84-TD4 to the acoustically transparent bodies U2-N08, U4-N08 and U5-N08 in SBP data (Fig. 5; Kioka et al., 2019a). The 59 cm-thick M082-TD2 was not previously mapped by Kioka et al. (2019a) and the relatively thinner U3-N08 does not have a correlative SBP-scale event deposit in M0084D. The upper (muddy) part of the thick U2-N08 body (equivalent to M84D-TD1) was previously cored and dated with bulk OC ^{14}C to be 1.77 ka (+0.49/−0.31) by Usami et al. (2021) and Schwestermann et al. (2021). Our equivalent SBP-scale deposit, M84D-TD1, can be correlated with M85-TD1, M88-TD1, and M86-TD2 along ITP4 based on similar physical property patterns (Fig. 9). This correlation cannot be further extended towards the south because no clear tie point to link between M0086B and M0087D (and thus between the Boundary Area and the Northern Japan Trench) could be identified. Yet, given our rough age estimates for the bottom of Hole M0087 in Basin C/N3 to be younger than 1.5 ka, even a theoretically-possible correlative ~1.77 ka event deposit would likely not have been reached at Site M0087D, and is not imaged in SBP data below the bottom of the Hole, because of low penetration depth of the acoustic signal in this boundary area (Figs. 6, 8).

Along the entire Northern Japan Trench (Basins N1-N3), the older SBP-scale event deposits generally correlate well to acoustically transparent bodies in SBP data and confirm the previous mapping and correlation by Kioka et al. (2019a). Similarly, we also correlate M84D-TD2 to the equivalent succession of high NGR values along N3-TP1 and use the average event-free sedimentation rate between Datum 2 (~1.77 ka) and Datum 3 (~11 ka) to estimate a depositional age of ~2.3 ka. This event horizon is also considered for M0088D by tentatively correlating M88D-TD2 with M84D-T2 along the event-base below the prominent NGR peak (dashed line in Fig. 9).

M84D-TD3 and M84-TD4 occur within the lower ~6 m of Hole M0084D where NGR is comparably lower. A similarly low NGR interval

occurs between ~11.5 and 14.5 mbsf in M0085D. Based on similar facies successions with different thicknesses but comparable physical property patterns, we correlate M84D-TD3 to a < 50 cm facies succession at ca. 12 mbsf in M0085D (defining N3-TP2), and M84D-TD4 with M85D-TD2 (defining N3-TP3 at the top since the base of M84D-TD4 is not recovered). Using the average event-free sedimentation rate between Datum 2 (~1.77 ka) and Datum 3 (~11 ka) (Table 3), we estimate N3-TP2 (=84D-TD3) to be ~5.8 ka and N3-TP3 (= 84D-TD4 = 85D-TD2) to be ~6.2 ka (Table 2). Estimated depositional ages of the older event deposit M85D-T3 is ~10.5 ka.

SBP-to-Core correlation at Site M0084 reveals that the ~6.2 ka 84D-TD4 corresponds to the uppermost part of the up-to 6 ms-TWT thick acoustically-transparent body U5-N08, identified and already proposed to correlate with U3-N05 in Basin N2 by Kioka et al. *(2019a)*. This correlation is confirmed by SBP-to-Core correlation at Site M0088D clearly linking top and bottom of the 5.6-m-thick 88D-TD3 with high-amplitude reflections at the top and base of U3-N05 (Fig. 8), and by similar pattern recognition in lithological and physical property data measured in the top of M84D-TD4 and M88D-TD3 and their similar overlying sequence (Fig. 9). Hence, we consider M88D-TD3 to represent the same ~6.2 ka event, and note that our new estimated event age, constraint by initial biostratigraphy results at Site M0085D where the entire Holocene stratigraphic sequences was recovered, refines the previous age of ~12.7 (+3.4/−1.9) ka estimated by Kioka et al., 2019a to a significantly younger age.

5. Discussion

IODP Expedition 386 marked the first utilization of giant piston coring within scientific ocean drilling to comprehensively investigate the deep subsurface of a hadal oceanic trench, acting as a depositional sink for earthquake-triggered sediment remobilization processes at a subduction zone. The herein presented results of IODP shipboard data analysis now establishes event-stratigraphic correlations of thick event beds across all 15 Expedition 386 Sites (Fig. 9). In the following section, we discuss the results with respect to advantages and limitations of the giant piston coring approach and here-applied methodology for event stratigraphy (5.1). We then consider the results of testing the previously published predictions of earthquake-related event deposits in SBP data (Kioka et al., 2019a) (section 5.2). Finally, we consider the results of our spatio-temporal event mapping with respect to the variable along-trench seismotectonic setting (section 5.2) and the potential for the entire IODP data set to address overarching submarine paleoseismology objectives at the Japan Trench (section 5.3).

5.1. Advantages and limitations of IODP giant piston coring

In comparison to the classical drilling approach, the major advantage of giant piston coring within IODP is to efficiently sample short but multiple cores and sites in ultra-deep-water environments. As proven successful by IODP Expedition 386, comparably cheap MSP-GPC operations can efficiently achieve margin-wide sampling at multiple sites in ultra-deepwater environments. Within internationally coordinated IODP science parties results from analyses conducted by a broad range of techniques from different disciplines can be efficiently integrated temporally and spatially to address high-level scientific objectives that cannot be addressed by smaller research groups on national levels.

The long cores also have some challenges that are inherently different to normal IODP drilling operations and that had implications in establishing the here-in presented core-to-SBP and event-stratigraphic correlations. One disadvantage of the GPC is the nonrecovery of the first up to 2–3 m of the uppermost subseafloor section, a common phenomenon for (giant) piston coring operations (e.g., Stow and Aksu, 1978; Buckley et al., 1994; Széréméta et al., 2004; Jutzeler et al., 2014). This results from free fall to the seabed and penetration into the seafloor by the heavy weight of the head and the main coring barrel of the piston corer disturbs the seabed and the uppermost subseafloor section. Although the mudline (water/sediment contact at the actual seafloor) is recovered by the trigger corer, pilot cores often were not long enough to include clear tie-points that allow stratigraphic correlation between the pilot cores and the long GPC, so that the core-depth scale of the long GPC remains a "floating" core-depth scale, with unknown gap at the top (Strasser et al., *2023*).

Another challenge impacting precise core-depth information is the partly severe coring disturbance (expansion/contraction) because of gas expansion and elastic rebound from recovering sedimentary section from ultra deep-water environment. In the Japan Trench hadal trench-fill, significant amounts of methane are produced by microbial methanogenesis in shallow subsurface depth (the SMTZ depth ranging from ~5.5 to 15 mbsf; Strasser et al., *2023*), due to the intense degradation of organic matter, which is linked to the emplacement of thick event deposits (Chu et al., 2023). Gas release and expansion of cored subsurface sequences with variable gas content at different in situ depth are amplified during decompression upon retrieval of one single 40 m GPC-barrel recovered from >7000 mbsl. This results in more severe differential depth-shifts within the barrel, compared to classical 9 m or shorter barrels in typical drilling operations at shallower water depths and where top and bottom depth of the core is known from the length of the drilling pipe below the seafloor. Since true penetration depth of the GPC barrel cannot be constrained from coring operation parameters, the effect of degassing and resulting depth shift within the GPC core barrel cannot be quantified. Voids resulting from degassing are frequently reported at the bottom and below thick event deposits (Strasser et al., *2023*), suggesting that thick event deposits decompressed differently than underlying and overlying "background" intervals. Furthermore, high gas content in the cores prohibited successful P-wave measurement (Strasser et al., *2023*). With the additional disadvantage (compared to standard scientific drilling operations) of not having downhole logging data available in GPC operations, the lack of a clearly defined core-depth to in situ-depth relation and missing p-wave velocity jeopardize standard depth-to-velocity transformation and core-log-seismic integration.

5.2. Validation of SBP-scale event-stratigraphy

Despite the limitations discussed above, our method of applying different velocities to different core intervals to establish core-to-SBP correlations has proven to be a reasonable solution. Our results reveal clear links between identified SBP-scale event deposits in IODP GPC cores and acoustically transparent bodies with lateral pinch-out geometries, as well as correlations between other stratigraphic marker horizons and high-amplitude reflections or intervals (Figs. 4–8). In fact, all SBP-scale event deposits identified in the studied holes show clear expressions in SBP data. Of these event beds, 49 % correspond exactly with SBP-units previously mapped by Kioka et al. (2019a) (Table 4). For the other 51 % of SBP-scales event beds identified in the cores (80 % of which are <1 m in thickness), we note correlative thin acoustically-transparent bodies with apparent onlaps towards the margins and intercalated between high-amplitude horizons in SBP-data, for which SBP-based seismic interpretation alone would be non-unique (and hence was not previously mapped (c.f. method definition for mapping SBP units by Kioka et al., *2019a*)). Only three SBP-units mapped by *Kioka* et al. (2019a; U5-S01 in the southernmost Japan Trench basin S1, and U2-N05 and U3-N08 in the northern basins N2 and N3) were not validated by SBP-scale event beds in the cores (Table 4). For the U5-S01 in the southern basin, however, a potentially correlative event bed is <50 cm thick in M0081D, potentially due to the challenges of establishing the "true" in situ thickness of the event deposits from core data. Hence, we conclude that SBP-scale event-stratigraphy on IODP cores almost perfectly validates the SBP-based event-bed mapping by Kioka et al. (2019a) and refines seismic interpretation also for event beds in the 0.5 to 1 m thickness range.

The differences in thickness between correlative SBP-units

Table 4
comparision to Kioka et al., 2019a.

Basin	SBP-scale event	Thickness (m)	Age estimate (a)	SBP Unit (Kioka et al., 2019a, 2019b)	Maximun thickness (m)	age estimated (ka) from core / *from correlation*	Test SBP prediction with core data (1) clear positive correlation (2) possible SBP-unit confirmed by coring (3) thin SBP-unit, but below SBP-scale in cores (4) test failed	Difference thickness TD and SBP-unit (m) (footnote 1)	Difference in age (ka)
	(this study)			(Kioka et al., 2019a)					
Southern Japan Trench									
S1	recoverd only in pilot core			U1-S01	3.7	2011 CE	n.a.		
	M81D-TD1	1.098	young than 869 CE	U2-S01	1		1	−0.098	
	M81D-TD2	0.95	young than 869 CE	U3-S01	2.6	1677 CE	1	1.65	
	M81D-TD3	1.468	young than 869 CE	not concluciveley identified in SBP data			2		
	M81D-TD4*	4.093	1081 (869 CE)	U4-S01	3.4	869 CE	1	−0.693	
	M81D-TD5	0.66	1.11	not concluciveley identified in SBP data			2		
	M81D-TD6	1.185	1.25	not concluciveley identified in SBP data			2		
	M81D-TD7	1.26	3.46	not concluciveley identified in SBP data			2		
	M81D-TD8	0.65	4.18	not concluciveley identified in SBP data			2		
	potentially correlative event deposits <50 cm			U5-S01	1.4	3.39	3		
S2	M95D-TD1	0.8949	young than 869 CE	not concluciveley identified in SBP data			2		
	M95D-TD2*	1.13	1081 (869 CE)	U1-S09	1.3	869 CE	1	0.17	
S2	recoverd only in pilot core			U1-S10	1.4	2011 CE	n.a.		
	M92D-TD1	0.95	young than 869 CE	U2-S10	1.4		1	0.45	
	M92D-TD2	1.258	young than 869 CE	U3-S10	1.5		1	0.242	
	M92D-TD3	0.653	young than 869 CE	included in the upper part of U-S10			2		
	M92D-TD4*	2.677	1081 (869 CE)	U4-S10	1.7	869 CE	1	−0.977	
S3	recoverd only in pilot core			U1-S15	1.2		n.a.		
	M91D-TD1	1.16	young than 869 CE	U2-S15	0.9	AD1454/1611	1	−0.26	
	M91D-TD2	0.8663	young than 869 CE	not concluciveley identified in SBP data			2		
	M91D-TD3*	4.345	1081 (869 CE)	U3-S15	3.6	869 CE	1	−0.745	
	M91D-TD4	1.347	2.99	U4-S15	1.6	2.25	1	0.253	−0.74
	M91D-TD5	0.95	5.18	U5-S15	1.6	4.02	1	0.65	−1.16
Central Japan Trench									
C1	No SBP-scale event beds			no SBP unit					
C2	No SBP-scale event beds			no SBP unit					
C2	recoverd only in pilot core			U1-C07	1.1		n.a.		
	M83F-TD1	6.94	young than 869 CE	U2-C07	5.4		1	−1.54	
	M83F-TD2*	4.26	1081 (869 CE)	U3-C07	4.3		1	0.04	
	M83F-TD3	0.525	3.34	not concluciveley identified in SBP data			2		
	M83F-TD4	1.135	5.68	U4-C07	2	3.8–4.9	1	0.865	
	M83F-TD5	0.87	5.92	not concluciveley identified in SBP data			2		
Central/Northern Japan Trench									
C/N1	recoverd only in pilot core			U1-C12			n.a.		
	M93B-TD1	3.977	0.69	U2-C12	3.2		1	−0.777	
	M93B-TD2	0.648	1.81	not concluciveley identified in SBP data			2		

(*continued on next page*)

Table 4 (*continued*)

Basin	SBP-scale event	Thickness (m)	Age estimate (a)	SBP Unit (Kioka et al., 2019a, 2019b)	Maximun thickness (m)	age estimated (ka) from core / *from correlation*	Test SBP prediction with core data (1) clear positive correlation (2) possible SBP-unit confirmed by coring (3) thin SBP-unit, but below SBP-scale in cores (4) test failed	Difference thickness TD and SBP-unit (m) (footnote 1)	Difference in age (ka)
	(this study)			(Kioka et al., 2019a)					
	M93B-TD3	0.64	1.89	not concluciveley identified in SBP data			2		
	M93B-TD4	0.53	2.46	not concluciveley identified in SBP data			2		
	M93B-TD5	0.53	3.26	not concluciveley identified in SBP data			2		
	M93B-TD6	1.986	3.29	U3-C12	1.8		1	−0.186	
	M93B-TD7	1.142	4.23	U4-C12	1.9		1	0.758	
	M93B-TD8	0.693	4.29	not concluciveley identified in SBP data			2		
	M93B-TD9	0.51	5.38	not concluciveley identified in SBP data			2		
	M93B-TD10	1.02	6.29	not concluciveley identified in SBP data			2		
C/N2	M94B-TD1	0.735	0.16	not concluciveley identified in SBP data			2		
	M94B-TD2	0.782	0.31	not concluciveley identified in SBP data			2		
	M94B-TD3	0.81	0.46	not concluciveley identified in SBP data			2		
	M94B-TD4	0.949	0.49	not concluciveley identified in SBP data			2		
	M94B-TD5	6.255	0.52	U1-C14	5.1		1	−1.155	
	M94B-TD6	0.52	0.84	not concluciveley identified in SBP data			2		
	M94B-TD7	0.539	0.96	not concluciveley identified in SBP data			2		
	M94B-TD8	0.97	0.99	not concluciveley identified in SBP data			2		
	M94B-TD9	0.952	1.13	not concluciveley identified in SBP data			2		
	M94B-TD10	2.404	1.46	not concluciveley identified in SBP data			2		
C/N3	recoverd only in pilot core			U1-C15	0.7		n.a.		
	M87D-TD1	3.02	0.13	U2-C15	3.3		1	0.28	
	M87D-TD2	0.943	0.15	not concluciveley identified in SBP data			2		
	M87D-TD3	1.09	0.63	not concluciveley identified in SBP data			2		
	M87D-TD4	2.62	0.65	U3-C15	3.1		1	0.48	
	M87D-TD5	0.783	0.66						
	M87D-TD6	0.636	0.75	U4-C15	3.8		1	−0.54	
	M87D-TD7	4.34	0.76						
	M87D-TD8	1.03	0.77	not concluciveley identified in SBP data			2		
	M87D-TD9	0.69	0.77	not concluciveley identified in SBP data			2		
	M87D-TD10	0.7	0.81	not concluciveley identified in SBP data			2		
	M87D-TD11	0.534	0.90	not concluciveley identified in SBP data			2		
	M87D-TD12	1.365	1.05	U5-C15	1.7		1	0.335	
	M87D-TD13	0.54	1.21	not concluciveley identified in SBP data			2		
	M87D-TD14	2.095	1.21	U6-C15	5.4		1	0.176	
	M87D-TD15	3.129	1.21						

(*continued on next page*)

Table 4 (*continued*)

Basin	SBP-scale event	Thickness (m)	Age estimate (a)	SBP Unit (Kioka et al., 2019a, 2019b)	Maximun thickness (m)	age estimated (ka) from core / *from correlation*	Test SBP prediction with core data (1) clear positive correlation (2) possible SBP-unit confirmed by coring (3) thin SBP-unit, but below SBP-scale in cores (4) test failed	Difference thickness TD and SBP-unit (m) (footnote 1)	Difference in age (ka)
	(this study)			(Kioka et al., 2019a)					
Northern Japan Trench									
N1	M86B-TD1	0.923	–	U1-N03	1.4		1	0.477	
	M86B-TD2**	10.098	1.77	U2-N03	8.4	2–3 century CE	1	−1.698	
N2	M88D-TD1**	12.924	1.77	U1-N05	9.6	2–3 century CE	1	−3.324	
	M88D-TD2	0.628	2.31	not conclucively identified in SBP data			2		
	no thick correlative event bed in cores			U2-N05	2.1		4		
	M88D-TD3	5.612	–	U3-N05	8.1		1	2.488	
N3	recoverd only in pilot core			U1-N08		1968 CE/1896 (?)	n.a.		
	M84D-TD1**	15.17	1.77	U2-N08		2–3 century CE	1		
	M84D-TD2	0.67	2.31	not conclucively identified in SBP data			2		
	no thick correlative event bed in cores			U3-N08	1.5	7.96	1		
	M84D-TD3	2.03	5.76	U4-N08	2.3	10.77	1	0.27	
	M84D-TD4	1.28	6.21	U5-N08	5.8	12.7	1	4.52	

NB: * = SBP-scale event beds correlated to the 869 CE Jogan earthquake. ** = SBP-scale event beds correlated to 1.77 ka.
footnote 1: note difference in defining thick event deposits in SBP data (≥ thicker than 2 times the vertical resolution (~ 40 cm in depth converted SBP data; Kioka et al., 2019a) and cores (>50 cm; *this study*). The cores experienced significant elastic decompression and gas expansion so the depth scale of the cores is relatively expanded to the in situ depth imaged in SBP data (see discussion in section 5.1). This justifies the larger thickness threshold "SBP-scale" event deposits in the cores, but introduces further uncertainties for the absolut values).

(estimated by Kioka et al. *(2019a))* and event-bed thickness in IODP cores (this study) are less than +/− 1 m for 80 % of identified beds, with larger discrepancies (+4.5 and − 3.3 m) for the thickest event beds. The latter can mostly be explained by the inherent uncertainties of measuring core-interval vs. "true" in situ thickness and of estimating p-wave velocity. This result further justifies our applied methodology of manually adjusting the core-depth scale within thick event-bed sequences between two correlation tie-points to visually fit marker horizons in the SBP data to be reasonable. As a result, here-presented Core-SBP correlation reveal quantitative means to better constrain the coring gap at the top of the GPC, establish revised core-composite depth scales also correcting for expansion and compression, as well as to evaluate and estimate measured vs. in-situ physical properties, respectively. Together with our findings that event-bed thickness generally decreases with increasing burial depth (Table 1; c.f. Basins S1, C2, N1–3), this will allow testing processed-based hypotheses of compaction (dewatering and consolidation) of event deposits with increasing burial depth and/or repeated of occurrence of earthquakes ("seismic strengthening hypothesis" Sawyer and DeVore, 2015), as we report.

The validation of SBP event stratigraphy predictions by identifying and correlating SBP-scale event deposits in the IODP cores, along with site-to-site correlations between Holes sampled in basin depocenter (expanded sequence) and basin margin (condensed sequence) also proves success of the 'composite-stratigraphy concept'. For all SBP-scale event deposits in the basin, correlative thinner event beds (<50 cm) with comparable facies and mostly identical pattern in physical properties (e.g., high MS/high NGR, high MS/low NGR, low MS/high NGR; generally decreasing-upwards above a sharp base) were identified. This significant difference in event bed thickness between basin and margin sites results from difference in the thickness of the fine-grained, mostly structureless intervals with homogenous physical properties. These intervals can be several meters thick in the basin depocenter and define the SBP-unit with its acoustically-transparent facies and lateral pinch-outs, but are only few cm to decimetre thick in the condensed sections. In contrast, the differences in interval thickness of "background" strata between SBP-scale event deposits (or between their correlative tie-points in the margin sites) are significantly smaller and are hypothesized to become neglectable (i.e., constant hemipelagic background sedimentation rates) once the stratigraphic sequences will be interrogated on the cm-scale to identify and map all event-deposits. Applying more detailed facies analyses for full-scale event stratigraphy will also benefit from the composite stratigraphy approach to accurately discriminate between event tops and overlying hemipelagic sequences by comparing turbidites-tail vs. bioturbation microfacies in the expanded and condensed section to precisely define and interpret the top of a single event vs. an event sequence vs. multiple independent events shortly after each other.

Last but not least, our results considering initial age constraints from shipboard radiolarian biostratigraphy support the "composite stratigraphy" hypothesis that the condensed sections comprise complete event stratigraphic sections reaching further back in time that can be better dated by applying more precise dating techniques (e.g., tephrochronology Ikehara et al., 2017b, PSV (Kanamatsu et al., *2022, 2023*), radiocarbon on specific compounds (Bao et al., 2018; Schwestermann et al., 2021; Chu et al., 2023). Although we are reluctant to make concrete statements about SBP-scale event ages without additional age constraints, we provide estimated event ages based on linear interpolation between previously dated events <2 ka (Datums 1 and 2) and the ~11 ka Datum 3 from initial shipboard radiolarian biostratigraphy in basins S2, C1, C2, and N3. These ages suggest that the previous estimates by Kioka et al. (2019a); based solely on downward extrapolation of

sedimentation rates constrained by historical events) at the base of the sampled holes were slightly too young (by ~1 kyrs) in the southern Japan Trench and significantly too old (by ~6 kyrs,) in the northern Japan Trench.

5.3. Along-strike variability of spatio-temporal event inventories

The inter-basin tie-points shown in Fig. 9 for Expedition 386 cores demonstrate alongstrike correlations of event sequences that agree with those proposed by Kioka et al. (2019a). For example, the inferred 869 CE "Jogan" event deposit correlation among all studied basins in the Southern and Central Japan Trench is confirmed by IODP data along interbasin tie-point ITP1. As a result, we are now able to identify and characterize this event below SBP-scale in condensed stratigraphic sections at basin margin sites and in basins with small flow accumulation areas (e.g., Basin C1 – Site M0090). This will allow examination of along-strike micro-facies variations to refine understanding of the extent and depositional processes related to the 869 CE "Jogan" earthquake and tsunami.

Similarly, correlation of the ~1.77 ka event deposit across all studied basins of the Northern Japan Trench along ITP-4 confirms this prominent marker event bed to be the volumetrically largest individual sediment remobilization event reported in the entire Japan Trench (413 × 106 km^3 (+80/−30); Kioka et al., 2019a). Yet, no conclusive correlation of event stratigraphic successions or individual event beds between the Basin C/N 1–3 ("boundary area") and the Central or Northern Basins can currently be identified. This boundary area is uniquely structurally complex due to the subducting petit-spot volcano field (Hirano et al., 2006) on the incoming plate (Fujie et al., 2020). High escarpments (>1 km) along this part of the trench axis suggest gravitational collapse and landslides on the lowermost landward slope (Nakamura et al., 2020, *2023*). Our results and initial age estimates from basins C/N 2 and 3 support this given that the entire cored sequence is mostly composed of relatively young event deposits (< 1.7 kyrs). Thus, the "boundary area" represents the trench segment with overall highest bulk sedimentation rates and highest event frequency (at least with respect to (i) events resulting in SBP-scale deposit and (ii) for the last ~1.7 ka covered by IODP cores). Based on these observations and the documented dominant event-deposit facies type (clay-supported mud clasts with subrounded and irregular shapes resulting from deposition of cohesive flows), we infer submarine landslide processes as an important agent for sediment remobilization at the boundary area, corroborating interpretations derived from bathymetric and reflection-seismic data (Nakamura et al., 2020, *2023*).

Regarding along-strike variability of spatio-temporal event inventories on the margin-wide scale, the boundary area around 39.3–39.4°N marks the first-order separation between contrasting event frequency/thickness relations in the Southern-to-Central and the Northern Japan Trench. We report more frequent but comparably thinner event deposits in the Southern and Central Japan Trench, and fewer but thicker event beds in the Northern Japan Trench. Since event thickness generally decreases with increasing overburden (as discussed in 5.2; and, thus, fewer SBP-scale event deposits are identified in the deep subsurface by our here-applied approach), we cannot identify any older SBP-scale deposits that span several basins (between S1 and C2) like the 2011 CE, 1454 CE and or the 869 CE events in the South-and-Central Japan Trench. However, we report at least one outstanding stratigraphic interval that occurs in all Southern-and-Central Japan Trench basins and for which possible stratigraphic correlations is inferred along tie-points S1-TP7 to SP-TP1 and S2-TP2 to C1-TP1 to C2-TP5 (Fig. 9). This interval is characterized by at least two distinct <50 cm-thick sandy event beds with unique physical properties (sharp density peaks, markedly high MS and markedly low NGR,) that correspond to prominent high amplitude reflection in SBP data (Fig. 8, also labelled b´ in Figs. 4 and 5). In basins with higher-flow accumulation areas (e.g., Basins S1 andS3) the correlative interval shows evidence for thin-acoustically-transparent bodies with lateral pinch-outs between the high-amplitude reflection occurring at subsurface depths below the bottom of holes cored at Sites M0081, and M0091 (Figs. 4 (labelled b) and 8). Acknowledging the large spatial imprint (comparable to the historical events) and considering increased compaction at deeper subsurface depths, these events that occurred within short times may have remobilized comparable amounts of sediment as is reported for events during the historic period. Differences in the current age estimates (derived from linear interpolation between Datum 1 (869 CE) and Datum 3 (~11 ka) at Sites M0092, −90 and − 89) for inferred correlative tie-points S2-TP2 (~6.9 ka), C1-TP1 (~6.2 ka) and C2-TP5 (~6.5 ka) are large (up to >700 years; Table 4). However, given the uncertainty in the initial shipboard biostratigraphy results and the overly simplistic methodology of linearly interpolation to estimate event (>50 cm)-free average sedimentations rates, these discrepancies in estimated event ages do not reject the plausible correlation. In contrast, we consider our correlation to be robust and quantify the range of possible error in our current age estimates to possibly be as large as 700 years.

In the Northern segment, two older event horizons with correlative SBP-scale deposits in at least two basins are dated at ~2.3 ka and ~ 6.2 ka (Figs. 7 and 8; Table 1). The latter shows similar acoustic and lithofacies characteristics as the ~1.77 ka event. Considering dewatering and compaction by increasing burial depth that can explain the difference in thickness of the two event beds, we interpret that the ~6.2 ka event could represent a similar ~1.77 ka-type event, while the intercalated ~2.3 ka event represents a smaller or different type of event. Despite large uncertainties in the initial age estimates of these event-horizons with large spatial extents, it is interesting that we note outstanding events around 6-7 ka in both the Southern-and-Central, as well as in the Northern Japan Trench. As a result, we hypothesize that this period may represent a "high activity" phase in sediment remobilization processes affecting the Japan Trench from the very southern to the northernmost trench basins.

Here-presented stratigraphic correlations and initial age estimates also document several meter thick intervals comprising densely interbedded parallel-laminated sands that appear to become thicker towards the "boundary area" (i.e., the interval including C2-TP1; Fig. 9). Thus, we infer a period with very-frequent sediment-remobilization must have affected the central Japan Trench around ~2.1 ka (i.e. estimate age of C2-TP1). This event sequence does not have thick correlative SBP units (see label a in Fig. 5), as no thick interval with structureless fine-grained sediments and homogenous physical properties is developed. Kanamatsu et al. (2022, 2023) report the same characteristic lithofacies with markedly low MS values in sediment cores from the same area, and more precisely date it by PSV to 2.3 ka (+/− <100 yrs). Inferred stratigraphic correlation with this ~2.3 event sequence reveals that our mean age estimate for tie-point C2-TP1 (derived linear interpolation between Datum 1 (869 CE) and Datum 3 (~11 ka) at Site M0089) is likely slightly too young (Tables 2,3).

5.4. Challenges for extracting megathrust signals from event-stratigraphic sequences

Overall, our findings of correlative SBP-scale event deposits comprising characteristic facies succession with thick fine-grained, mostly structureless intervals with homogenous physical properties corresponding to acoustically-transparent bodies with lateral pinch-out geometries in SBP-data compare well with observations and data from other studies documenting similar seismic profiles, core data, and correlations of homogenous facies (often termed "homogenites" after Kastens and Cita (1981) that have been inferred as records of past earthquake occurrence (e.g. McHugh et al., 2020; Seibert et al., *2024*). On the full margins-scale, our results reveal distinctly different SBP-scale event stratigraphies for the trench segments north and south of the "boundary area" which is characterized by landslide scars on the lower trench-slope, relatively elevated trench-floor bathymetry and the

subduction of oceanic lithosphere affected by petit-spot volcanism. This difference supports the hypothesis that this structurally controlled divide may act as segment boundary of megathrust earthquakes (Fujie et al., 2020). In contrast, we observe no obvious difference in SBP-scale event stratigraphies between the Southern and Central Japan Trench, which span across the SW-NE-striking boundary in upper-plate structure (projected to near the trench axis; dashed line in Fig. 2) that is hypothesized to be another possible segment boundary (Bassett et al., 2016*)*.

In the southern to central Japan Trench, SBP-scale event stratigraphy rather seems to be related to flow-accumulation area, with larger volumes recorded in Basins with comparatively higher flow accumulation. This suggests that upslope catchment area links to the volume of surficial slope sediment that is mobilized by seismic ground shaking (McHugh et al., *2016*; Kioka et al., 2019a, 2019b; Schwestermann et al., *2021; 2022;* Ikehara et al., 2020). Yet, different portions of upslope areas may have different ground motion characteristics and/or different responses of slope sediments to earthquake shaking. These factors, alongside downcore compaction over time, can govern the thickness of potentially correlative event beds in respective trench-fill basins. As a result, our generic threshold definition of mapping >0.5 m thick deposits is perhaps too restrictive, since the lack of SBP-scale event deposits in a given stratigraphic interval does not imply actual absence of event deposits, as its thickness just may be below the threshold. Hence, we confirm that identification of event sequences at a higher resolution than the currently considered SBP-scale is required to test for spatial correlations and variability of event-deposits more accurately for sound paleoseismological interpretation.

Our positive correlations using tie-points at the sub-SBP-scale level clearly suggest that event-stratigraphies can be further examined by detailed facies analyses and further integration of high-resolution physical and chemical proxy data from core scanning and logging (e.g., Schwestermann et al., 2020). Strikingly, we document several event horizons that are characterized by distinctly different relations and values in MS and NGR. These unique characteristics may provide information on sediment provenance and therefore could be explored to resolve the different sources of sediment remobilization and test for the different scenarios affecting different upslope catchment areas and flow accumulation pathways (Fig. 2c; Schwestermann et al., 2020; McHugh et al., 2020; Usami et al., 2021).

For the southern Japan Trench, we further note that Basin S1 (Sites M0081/82) appears to record more event deposits within the same stratigraphic intervals compared to Basins S3 (Site M0091), which also has generally high-flow accumulation. The higher event frequency in the southernmost basin has already been documented for the historical period (Schwestermann et al., *2021*; Kioka et al., 2019*a*; Fig.1). Together, we infer that this observation and previous findings, suggest that Basin S1 records both megathrust rupture of the Tohoku asperity, as well as of the Izu asperity in the south (Fig. 2). Hence, detailed event stratigraphy on the (micro-)facies level is expected to resolve and allow for deconvolution of the mixed paleoseismologic signals in Basins S1 and S2 for megathrust rupture histories of the two different asperities.

A major limitation for any paleoseismological interpretation of the here-presented event-stratigraphy is the lack of accurate age control. Our initial age estimates using preliminary constraints from biostratigraphy imply that interrogation at the SBP-scale level is too simplistic to obtain event-free sedimentation rates that provide accurate event ages estimates. As a result, event horizons that we correlate based on examination of patterns in lithofacies and physical properties characteristics do not always overlap temporally. Hence, we hypothesize that a more detailed review aimed at more accurately defining event-free thicknesses at the lithofacies level, along with adding more robust and precise age constraints from other dating methods will constrain precise event ages so that the synchronicity criterion - as key for paleoseismological interpretation - can be evaluated and the along-strike correlations or variations can be more robustly explored.

In summary, initial shipboard data and thereof-derived event stratigraphic correlations on the SBP-scale, do not yet allow for conclusive paleoseismological interpretation. We therefore refrain from repeating and conceptually discussing the previously formulated hypothesis of megathrust segmentation and giant earthquake recurrence cycles at this stage (section 2). Instead, we posit that the vast and high-quality data set from IODP GPC for Expedition 386 and here-presented positive initial correlation results provide a strong foundation for more detailed studies to (i) more accurately define sediment provenance, (ii) further characterize event deposition dynamics on the micro-facies level, and (iii) constrain precise event ages to evaluate the synchronicity criterion in order to robustly test along-strike correlations and achieve the goal of extracting paleoseismic signals from the Japan Trench event stratigraphies.

6. Conclusions, implications, and future perspectives

IODP Expedition 386 was the first expedition to utilize giant piston coring (GPC) within IODP to sample the shallow subsurface at multiple sites with multiple holes along an axis-parallel transect spanning over 600 km across the entire Japan Trench subduction zone at a water depth of 7–8 km. The here-presented event-stratigraphy based on IODP cores confirms previously predicted earthquake-related event deposits identified using high-resolution hydro-acoustic subbottom profiler (SBP) data. The study suggests that the limitations of GPC in accurately measuring subsurface depth and thickness can be addressed through high-resolution core-to-SBP and core-to-core correlation, overcoming issues such as nonrecovery of the sediment-water interface and differential expansion/compaction of sediments from ultra deep-water sites.

From a scientific perspective, the successful correlation of SBP-scale event deposits across multiple sites spanning several basins over hundreds of kilometres provides the first comprehensive event stratigraphic record covering more than ten thousand years, documenting large-scale sediment remobilization events, likely related to subduction megathrust earthquakes, into the hadal oceanic trench. Key observations include variations in event frequency and thickness along the Japan Trench, with distinct differences between the Southern-to-Central and Northern regions, as well as increased submarine landslide activity in specific boundary areas.

While conclusive paleoseismological interpretations at a detailed level are not yet feasible, the study highlights the potential for further research utilizing sub-SBP scale marker horizons and ongoing post-expedition analyses of core data to enhance understanding of earthquake histories in the Japan Trench. Initial findings suggest that the submarine paleoseismology approach can be validated in the prehistoric context of the Japan Trench, paving the way for reconstructing long-term earthquake histories along the entire subduction zone.

CRediT authorship contribution statement

Michael Strasser: Writing – original draft, Validation, Methodology, Investigation, Conceptualization. **Ken Ikehara:** Writing – review & editing, Validation, Methodology, Investigation, Conceptualization. **Charlotte Pizer:** Writing – original draft, Visualization, Investigation. **Takuya Itaki:** Writing – review & editing, Investigation. **Yasufumi Satoguchi:** Writing – review & editing, Investigation. **Arata Kioka:** Writing – review & editing, Investigation. **Cecilia McHugh:** Writing – review & editing, Investigation. **Jean-Noel Proust:** Writing – review & editing, Investigation. **Derek Sawyer:** Writing – review & editing, Investigation. **IODP Expedition 386 Management Team** *(J. Everest, L. Maeda, K. Hochmuth, H. Grant, M. Stewart, N. Okutsu, N. Sakurai, T. Yokoyama)*: Resources - Data Curation - Project administration. **IODP Expedition 386 Science Party** *(R. Bao, P. Bellanova, M. Brunet, Z. Cai, A. Cattaneo, K.H. Hsiung, J.-J.S. Huang, T. Ishizawa, K. Jitsuno, J.E. Johnson, T. Kanamatsu, M. Keep, M. Kölling, M. Luo, C. März, A. Micallef, Y. Nagahashi, D. Pandey, T. Rasbury, N. Riedinger, C. Seibert, M. Silver, S.*

Straub, J.J. Virtasalo, Y.H. Wang, T.-W. Wu, S.D. Zellers): Investigation.

Declaration of competing interest

There are no competing interests to declare.

Data availability

All IODP mission-specific platform data are accessible at http://iodp.pangea.de. Hydroacoustic data reused from Kioka et al., 2019a are available at Bundesamt für Seeschifffahrt und Hydrographie (https://www.bsh.de/DE/Home/home_node.html) and JAMSTEC-DARWIN database (http://www.godac.jamstec.go.jp/darwin/e).

Acknowledgment

This study used samples and data provided by the International Ocean Discovery Program (IODP). We thank the technical staff and crews of IODP Expedition 386. This research was funded in part by the Austrian Science Fund (FWF)[grant https://doi.org/10.55776/P36809 to M.S]. For open access purposes, the author has applied a CC BY public copyright license to any author accepted manuscript version arising from this submission We acknowledge editorial handling and constructive comments by guest editor Angelo Camerlenghi and two anonymous reviewers that helped to improve the manuscript.

Appendix A. Supplementary data

Supplementary data to this article can be found online at https://doi.org/10.1016/j.margeo.2024.107387.

References

Bao, R., et al., 2018. Tectonically-triggered sediment and carbon export to the Hadal zone. Nat. Commun. 9, 121. https://doi.org/10.1038/s41467-017-02504-1.
Barbot, S., 2020. Frictional and structural controls of seismic super-cycles at the Japan trench. Earth Planets Space. https://doi.org/10.1186/s40623-020-01185-3.
Bassett, D., et al., 2016. Upper-plate controls on co-seismic slip in the 2011 Tohoku-oki earthquake. Nature. https://doi.org/10.1038/nature16945.
Bilek, S., Lay, T., 2018. Subduction zone megathrust earthquakes. Geosphere. https://doi.org/10.1130/GES01608.1.
Buckley, D.E., MacKinnon, W.G., Cranston, R.E., Christian, H.A., 1994. Problems with piston core sampling: mechanical and geochemical diagnosis. Mar. Geol. 117 (1–4), 95–106. https://doi.org/10.1016/0025-3227(94)90008-6.
Chu, M., Liu, J., Li, H., Zhou, Y., Wang, N., Xia, C., Kopf, A., Strasser, M., Bao, R., 2023. Earthquake-induced redistribution and reburial of microbes in the hadal trenches. Innov. Geosci. 1 (2), 100027 https://doi.org/10.59717/j.xinn-geo.2023.100027.
Daigle, H., Duarte, J.C., Fagereng, A., Paris, R., Persaud, P., Gómez-García, Á.M., the Lisbon MagellanPlus Workshop Participants, 2023. MagellanPlus Workshop: mission-specific platform approaches to assessing natural hazards that impact society. Sci. Drill. 32, 101–111. https://doi.org/10.5194/sd-32-101-2023.
De Batist, M., Talling, P., Strasser, M., Girardclos, S., 2017. Subaquatic paleoseismology: records of large Holocene earthquakes in marine and lacustrine sediments. Mar. Geol. 384, 1–3. https://doi.org/10.1016/j.margeo.2017.04.010.
DeMets, C., Gordon, R.G., Argus, D.F., 2010. Geologically current plate motions. Geophys. J. Int. 181 (1), 1–80. https://doi.org/10.1111/j.1365-246X.2009.04491.x.
Fujie, G., et al., 2020. Spatial variations of incoming sediments… Implications for megathrust eq. Geology. https://doi.org/10.1130/G46757.1.
Goldfinger, C., Nelson, C.H., Morey, A.E., Johnson, J.E., Patton, J.R., Karabanov, E.B., Gutierrez-Pastor, J., Eriksson, A.T., Gracia, E., Dunhill, G., Enkin, R.J., Dallimore, A., Vallier, T., 2012. Turbidite event history—methods and implications for Holocene paleoseismicity of the Cascadia subduction zone. In: USGS Professional Paper, 1661-F. https://doi.org/10.3133/pp1661F.
Goto, et al., 2019. Tsunami history over the past 2000 years on the Sanriku coast, Japan. Sediment. Geol. https://doi.org/10.1016/j.sedgeo.2019.01.001.
Goto, et al., 2021. Ten years after the 2011 Tohoku-oki earthquake and tsunami. Earth-Sci. Rev. https://doi.org/10.1016/j.earscirev.2020.103417.
Grácia, E., Vizcaino, A., Escutia, C., Asioli, A., Rodés, Ü., Pallàs, R., Garcia-Orellana, J., Lebreiro, S., Goldfinger, C., 2010. Holocene earthquake record offshore Portugal (SW Iberia): testing turbidite paleoseismology in a slow-convergence margin. Quat. Sci. Rev. 29 (9–10), 1156–1172. https://doi.org/10.1016/j.quascirev.2010.01.010.
Higaki, H., et al., 2021. Three thousand year paleo-tsunami history of the southern part of the JT. Prog. Earth Planet Sci. https://doi.org/10.1186/s40645-021-00415-w.
Hirano, N., Takahashi, E., Yamamoto, J., Abe, N., Ingle, S.P., Kaneoka, I., Hirata, T., Kimura, J.-I., Ishii, T., Ogawa, Y., Machida, S., Suyehiro, K., 2006. Volcanism in response to plate flexure. Science 313 (5792), 1426–1428. https://doi.org/10.1126/science.1128235.
Howarth, J.D., Orpin, A.R., Kaneko, Y., Strachan, L.J., Nodder, S.D., Mountjoy, J.J., Barnes, P.M., Bostock, H.C., Holden, C., Jones, K., Cağatay, M.N., 2021. Calibrating the marine turbidite palaeoseismometer using the 2016 Kaikōura earthquake. Nat. Geosci. 14 (3), 161–167. https://doi.org/10.1038/s41561-021-00692-6.
Hussong, et al., 1982. Deep Sea Drilling Project Leg 60: Cruise Objectives, Principal Results, and Explanatory Notes. https://doi.org/10.2973/dsdp.proc.60.101.1982 http://deepseadrilling.org/60/dsdp_toc.htm.
Ikehara, et al., 2016. Documenting large earthquakes similar to the 2011 Tohoku-oki earthquake. Earth Planet. Sci. Lett. https://doi.org/10.1016/j.epsl.2016.04.009.
Ikehara, et al., 2017a. Spatial variability in sediment lithology and processes along the JT. Geol. Soc. Lond., Spec. Publ. https://doi.org/10.1144/SP456.9.
Ikehara, et al., 2017b. Three important Holocene tephras off the Pacific coast of the Tohoku region. Quat. Int. https://doi.org/10.1016/j.quaint.2017.08.022.
Ikehara, K., Usami, K., Kanamatsu, T., 2020. Repeated occurrence of surface-sediment remobilization along the landward slope of the Japan Trench by great earthquakes. Earth Planets Space 72 (1), 114. https://doi.org/10.1186/s40623-020-01241-y.
Ikehara, et al., 2021. Characteristics and distribution of the event deposits induced by the 2011 Tohoku. Sediment. Geol. https://doi.org/10.1016/j.sedgeo.2020.105791.
Ikehara, K., Strasser, M., Everest, J., Maeda, L., Hochmuth, K., the Expedition 386 Scientists, 2023. Expedition 386 preliminary report: Japan Trench paleoseismology. Int. Ocean Discov. Prog. https://doi.org/10.14379/iodp.pr.386.2023.
Ishizawa, et al., 2022. Paleotsunami history along the northern Japan trench based on sequential dating. Quat. Sci. Rev. https://doi.org/10.1016/j.quascirev.2022.107381.
Itaki, T., et al., 2009. Late Pleistocene stratigraphy and palaeoceanographic implications in northern Bering Sea slope sediments: evidence from the radiolarian species Cycladophora davisiana. J. Quat. Sci. 24 (8), 856–865. https://doi.org/10.1002/jqs.1356.
Jamieson, A.J., Fujii, T., Mayor, D.J., Solan, M., Priede, I.G., 2010. Hadal trenches: the ecology of the deepest places on Earth. Trends Ecol. Evol. 25 (3), 190–197. https://doi.org/10.1016/j.tree.2009.09.009.
Jutzeler, M., White, J.D.L., Talling, P.J., McCanta, M., Morgan, S., Le Friant, A., Ishizuka, O., 2014. Coring disturbances in IODP piston cores with implications for offshore record of volcanic events and the Missoula megafloods. Geochem. Geophys. Geosyst. 15 (9), 3572–3590. https://doi.org/10.1002/2014GC005447.
Kanamatsu, et al., 2022. Stratigraphy of deep-sea marine sediment using paleomag. secular variation. Mar. Geol. https://doi.org/10.1016/j.margeo.2021.106669.
Kanamatsu, T., Ikehara, K., Hsiung, K.H., 2023. Submarine paleoseismology in the Japan Trench of northeastern Japan: turbidite stratigraphy and sedimentology using paleomagnetic and rock magnetic analyses. Prog. Earth Planet Sci. 10, 16. https://doi.org/10.1186/s40645-023-00545-3.
Kanamori, H., 1971. Seismological evidence for a lithospheric normal faulting — the Sanriku earthquake of 1933. Phys. Earth Planet. Inter. 4, 289–300. https://doi.org/10.1016/0031-9201(71)90013-6.
Kastens, K.A., Cita, M.B., 1981. Tsunami-induced sediment transport in the abyssal Mediterranean Sea. GSA Bull. 92 (11), 845–857. https://doi.org/10.1130/0016-7606(1981)92<845:tstita>2.0.co;2.
Kioka, A., Strasser, M., 2022. Oceanic trenches. In: Shroder, J.F. (Ed.), Treatise on Geomorphology, , Second edition8, pp. 882–900. https://doi.org/10.1016/B978-0-12-818234-5.00167-X.
Kioka, A., Schwestermann, T., Moernaut, J., Ikehara, K., Kanamatsu, T., Eglinton, T.I., Strasser, M., 2019a. Event stratigraphy in a hadal oceanic trench: the Japan Trench as sedimentary archive recording recurrent giant subduction zone earthquakes and their role in organic carbon export to the deep sea. Front. Earth Sci. 7, 319. https://doi.org/10.3389/feart.2019.00319.
Kioka, A., Schwestermann, T., Moernaut, J., Ikehara, K., Kanamatsu, T., McHugh, C.M., dos Santos Ferreira, C., Wiemer, G., Haghipour, N., Kopf, A.J., Eglinton, T.I., Strasser, M., 2019b. Megathrust earthquake drives drastic organic carbon supply to the hadal trench. Sci. Rep. 9 (1), 1553. https://doi.org/10.1038/s41598-019-38834-x.
Kodaira, et al., 2021. Investigating a tsunamigenic megathrust earthquake in the Japan Trench. Science. https://doi.org/10.1126/science.abe1169.
McHugh, C.M., Kanamatsu, T., Seeber, L., Bopp, R., Cormier, M.-H., Usami, K., 2016. Remobilization of surficial slope sediment triggered by the A.D. 2011 Mw 9 Tohoku-Oki earthquake and tsunami along the Japan Trench. Geology 44 (5), 391–394. https://doi.org/10.1130/G37650.1.
McHugh, C.M., Seeber, L., Rasbury, T., Strasser, M., Kioka, A., Kanamatsu, T., Ikehara, K., Usami, K., 2020. Isotopic and sedimentary signature of megathrust ruptures along the Japan subduction margin. Mar. Geol. 428, 106283 https://doi.org/10.1016/j.margeo.2020.106283.
McInroy et al. 2024, this volume.
Moernaut, J., 2020. Time-dependent recurrence of strong earthquake shaking near plate boundaries. Earth Sci. Rev. https://doi.org/10.1016/j.earscirev.2020.103344.
Molenaar, A., et al., 2019. Earthquake impact on active margins: Tracing surficial remobilization. Geophys. Res. Lett. https://doi.org/10.1029/2019GL082350.
Morley, J.J., et al., 1982. Stratigraphic framework for the late Pleistocene in the Northwest Pacific Ocean. Deep Sea Res. Part A Oceanogr. Res. Pap. 29 (12), 1485–1499. https://doi.org/10.1016/0198-0149(82)90038-3.
Nagai, R., Kikuchi, M., Yamanaka, Y., 2001. Comparative study on the source processes of recurrent large earthquakes in Sanriku-oki Region: the 1968 Tokachi-oki earthquake and the 1994 Sanriku-oki earthquake. Zisin-II 54, 267–280. https://doi.org/10.4294/zisin1948.54.2_267 (in Japanese with English Abstract).
Nakamura, Y., Fujiwara, T., Kodaira, S., Miura, S., Obana, K., 2020. Correlation of frontal prism structures and slope failures near the trench axis with shallow megathrust slip

at the Japan Trench. Sci. Rep. 10 (1), 11607. https://doi.org/10.1038/s41598-020-68449-6.
Nakamura, Y., Kodaira, S., Fujie, G., et al., 2023. Incoming plate structure at the Japan Trench subduction zone revealed in densely spaced reflection seismic profiles. Prog. Earth Planet Sci. 10, 45. https://doi.org/10.1186/s40645-023-00579-7.
Nakanishi, et al., 2022. Holocene coastal evolution, past tsunamis, and extreme wave event. Mar. Geol. https://doi.org/10.1016/j.margeo.2021.106663.
Nakata, et al., 2021. Presence of interplate channel layer controls of slip during and after the 2011 EQ Scientific Report. https://doi.org/10.1038/s41598-021-86020-9.
Oguri, K., Kawamura, K., Sakaguchi, A., Toyofuku, T., Kasaya, T., Murayama, M., Fujikura, K., Glud, R.N., Kitazato, H., 2013. Hadal disturbance in the Japan Trench induced by the 2011 Tohoku–Oki Earthquake. Sci. Rep. 3 (1), 1915. https://doi.org/10.1038/srep01915.
Philibosian, Meltzner, 2020. Segmentation and supercycles: a catalog of earthquake rupture patterns. Quat. Sci. Rev. https://doi.org/10.1016/j.quascirev.2020.106390.
Pilarczyk, et al., 2021. A further source of Tokyo earthquakes and Pacific Ocean tsunamis. Nat. Geosci. https://doi.org/10.1038/s41561-021-00812-2.
Polonia, A., Nelson, C.H., Romano, S., Vaiani, S.C., Colizza, E., Gasparotto, G., Gasperini, L., 2017. A depositional model for seismo-turbidites in confined basins based on Ionian Sea deposits. Mar. Geol. 384, 177–198. https://doi.org/10.1016/j.margeo.2016.05.010.
Pouderoux, H., Proust, J.-N., Lamarche, G., 2014. Submarine paleoseismology of the northern Hikurangi subduction margin of New Zealand as deduced from turbidite record since 16 ka. Quat. Sci. Rev. 84, 116–131. https://doi.org/10.1016/j.quascirev.2013.11.015.
Satake, K., 2015. Geological and historical evidence of irregular recurrent earthquakes in Japan. Phil. Trans. R. Soc. A. https://doi.org/10.1098/rsta.2014.0375.
Sawai, Y., 2020. Subduction zone paleoseismology along the Pacific coast of Northeast Japan. Earth Sci. Rev. https://doi.org/10.1016/j.earscirev.2020.103261.
Sawai, Y., Namegaya, Y., Okamura, Y., Satake, K., Shishikura, M., 2012. Challenges of anticipating the 2011 Tohoku earthquake and tsunami using coastal geology. Geophys. Res. Lett. 39, L21309. https://doi.org/10.1029/2012GL053692.
Sawai, Y., Namegaya, Y., Tamura, T., Nakashima, R., Tanigawa, K., 2015. Shorter intervals between great earthquakes near Sendai: scour ponds and a sand layer attributable to A.D. 1454 overwash. Geophys. Res. Lett. 42, 4795–4800. https://doi.org/10.1002/2015GL064167.
Sawyer, DeVore, 2015. Elevated shear strength of sediments on active margins: evidence for seismic strengthening. Geophys. Res. Lett. https://doi.org/10.1002/2015GL066603.
Schwestermann, et al., 2020. Multivariate statistical and multi-proxy constraints on earthquake. Geochem. Geophys. Geosyst. 21 https://doi.org/10.1029/2019GC008861.
Schwestermann, et al., 2021. Event-dominated transport, provenance and burial of organic carbon. Earth Planet. Sci. Lett. https://doi.org/10.1016/j.epsl.2021.116870.
Seibert, et al., 2024. Sedimentary Records in the Lesser Antilles Fore-Arc Basins Provide Evidence of Large Late Quaternary Megathrust Earthquakes. https://doi.org/10.1029/2023GC011152.
St-Onge, G., Chapron, E., Mulsow, S., Salas, M., Viel, M., Debret, M., Foucher, A., Mulder, T., Winiarski, T., Desmet, M., Costa, P.J.M., Ghaleb, B., Jaouen, A., Locat, J., 2012. Comparison of earthquake-triggered turbidites from the Saguenay (Eastern Canada) and Reloncavi (Chilean margin) Fjords: implications for paleoseismicity and sedimentology. Sediment. Geol. 243–244, 89–107. https://doi.org/10.1016/j.sedgeo.2011.11.003.
Stow, D.A.V., Aksu, A.E., 1978. Disturbances in soft sediments due to piston coring. Mar. Geol. 28 (1–2), 135–144. https://doi.org/10.1016/0025-3227(78)90101-9.
Strasser, M., Kölling, M., Ferreira, C.D.S., Fink, H.G., Fujiwara, T., Henkel, S., Ikehara, K., Kanamatsu, T., Kawamura, K., Kodaira, S., Römer, M., Wefer, G., SO219A, R.V.S.C., and scientists, J.C.M.-E, 2013. A slump in the trench: tracking the impact of the 2011 Tohoku-Oki earthquake. Geology 41 (8), 935–938. https://doi.org/10.1130/G34477.1.
Strasser, M., Ikehara, K., Cotterill, C., 2019. Expedition 386 scientific prospectus: Japan Trench paleoseismology. Int. Ocean Discov. Prog. https://doi.org/10.14379/iodp.sp.386.2019.
Strasser, M., Ikehara, K., Everest, J., the Expedition 386 Scientists, 2023. . Japan Trench Paleoseismology. In: Proceedings of the International Ocean Discovery Program, 386. International Ocean Discovery Program, College Station, TX. https://doi.org/10.14379/iodp.proc.386.2023.
Strasser, M., Ikehara, K., Everest, J., the Expedition 386 Scientists, 2023. Japan Trench Paleoseismology. Proceedings of the International Ocean Discovery Program, 386. International Ocean Discovery Program, College Station, TX. https://doi.org/10.14379/iodp.proc.386.2023.
Széréméta, N., Bassinot, F., Balut, Y., Labeyrie, L., Pagel, M., 2004. Oversampling of sedimentary series collected by giant piston corer: evidence and corrections based on 3.5-kHz chirp profiles. Paleoceanography 19 (1). https://doi.org/10.1029/2002PA000795. PA1005.
Takada, K., Shishikura, M., Imai, K., Ebina, Y., Goto, K., Koshiya, S., Yamamoto, H., Igarashi, A., Ichihara, T., Kinoshita, H., Ikeda, T., 2016. Distribution and ages of tsunami deposits along the Pacific coast of the Iwate prefecture. Annual Rep. Active Fault Paleoearthquake Res. 16 (2016), 1–52 (in Japanese with English abstruct).
Takeuchi, H., Fuji, R., Mimura, N., Imamura, F., Satake, K., Tsuji, Y., et al., 2007. Survey of run-up height of Empo Boso-oki earthquake tsunami on the coast from Chiba prefecture to Fukushima prefecture. Rekishi-Jishin (Hist. Earthq.) 22, 53–59 (in Japanese with English Abstract).
Tanioka, Y., Satake, K., 1996. Fault parameters of the 1896 Sanriku Tsunami Earthquake estimated from Tsunami Numerical Modeling. Geophys. Res. Lett. 23, 1549–1552. https://doi.org/10.1029/96GL01479.
Uchida, Bürgmann, 2021. A decade of lessons learned from the 2011 Tohoku-Oki earthquake. Rev. Geophys. https://doi.org/10.1029/2020RG000713.
Uchida, N., Matsuzawa, T., 2011. Coupling coefficient, hierarchical structure, and earthquake cycle for the source area of the 2011 off the Pacific coast of Tohoku earthquake inferred from small repeating earthquake data. Earth Planets Space 63 (7), 30. https://doi.org/10.5047/eps.2011.07.006.
Ueda, H., Kitazato, H., Jamieson, A., et al., 2023. The submarine fault scarp of the 2011 Tohoku-oki Earthquake in the Japan Trench. Commun. Earth Environ. 4, 476. https://doi.org/10.1038/s43247-023-01118-4.
Usami, K., Ikehara, K., Kanamatsu, T., McHugh, C.M., 2018. Supercycle in great earthquake recurrence along the Japan Trench over the last 4000 years. Geosci. Lett. 5 (1), 11. https://doi.org/10.1186/s40562-018-0110-2.
Usami, K., Ikehara, K., Kanamatsu, T., Kioka, A., Schwestermann, T., Strasser, M., 2021. The link between upper-slope submarine landslides and mass transport deposits in the hadal trenche. In: Sassa, K., Mikoš, M., Sassa, S., Bobrowsky, P.T., Takara, K., Dang, K. (Eds.), Sendai Landslide Partnerships and Kyoto Landslide Commitment. Understanding and Reducing Landslide Disaster Risk, 1. https://doi.org/10.1007/978-3-030-60196-6_26.
Walton, et al., 2021. Toward an integrative geological + geophysical view of Cascadia subduction EQs. Annu. Rev. Earth Planet. Sci. https://doi.org/10.1146/annurev-earth-071620-065605.
Wirth, et al., 2022. The occurrence and hazards of great subduction zone earthquakes. Nat. Rev. Earth Environ. https://doi.org/10.1038/s43017-021-00245-w.